OPTIMIZATION OF MICRO WIRE ELECTRO DISCHARGE MACHINING PROCESS PARAMETERS USING AEROSPACE MATERIAL

A Thesis Submitted to

National Institute of Technology, Rourkela

In Partial fulfillment of the requirement for the degree of

Master of Technology

in

Mechanical Engineering

By

MANOJ KUMAR MOHANTA

Roll No. 211ME2351

Under the guidance and supervision of

Prof. K. P. MAITY

Department of Mechanical Engineering

National Institute of Technology

Rourkela -769 008 (India)

2013

National Institute of Technology

Rourkela

CERTIFICATE

This is to certify that the thesis entitled "**OPTIMIZATION OF MICRO WIRE ELECTRO DISCHARGE MACHINING PROCESS PARAMETERS USING AEROSPACE MATERIAL"** submitted to the National Institute of Technology, Rourkela by **MANOJ KUMAR MOHANTA, Roll No. 211ME2351** for the award of the Degree of Master of Technology in Mechanical Engineering with specialization in Production Engineering is a record of bonafide research work carried out by him under my supervision and guidance. The results presented in this thesis has not been, to the best of my knowledge, submitted to any other University or Institute for the award of any degree or diploma. The thesis, in my opinion, has reached the standards fulfilling the requirement for the award of the degree of Master of technology in accordance with regulations of the Institute.

Place: NIT Rourkela

Date:

Dr. K. P. Maity

HOD & Professor

Department of Mechanical Engineering

National Institute of Technology, Rourkela

ACKNOWLEDGEMENT

I would like to express my gratitude to my supervisor **Prof. K.P Maity** for the useful comments, remarks and engagement through the learning process of this master thesis. I am also grateful to **Prof. Sunil Kumar Sarangi**, director NIT Rourkela who took keen interest in the work. A special thanks goes to Ritanjali Sethy, who help me to understand and gave suggestion about the task "*PCA based optimizations*". A special gratitude I give to Mr. Kanhu Charan Nayak whose contribution in stimulating suggestions and encouragement helped me to coordinate my project especially in writing this report.

I am obliged to all my friends of NIT, Rourkela, for the valuable information provided by them in their respective fields. I am grateful for their cooperation during the period of my assignment.

Lastly, I thank almighty and my parents for their constant encouragement without which this assignment would not be possible.

Date: Manoj Kumar Mohanta

Place: Roll no: 211ME2351

Nomenclature

EDM	Electrical discharge machining
µWEDM	Micro Wire Electrical discharge machining
MRR	Material removal rate (mm^3/min)
Hi	heat input to the work piece
V	Voltage (V)
I	Current (Amp)
Q(r)	Heat flux (W/m^2)
R	Spark radius (µm)
K	Thermal conductivity (W/mK)
T	Temperature variable (K)
T0	Initial temperature (K)
Ton	Spark-on time (µs)
Toff	Spark-off time (µs)
x,y	Cartesian coordinate of work piece
Cp	Specific heat (J/kgK)
Cv	Crater volume (µm3)
PCA	Principal Component Analysis
GRA	Grey Relational Analysis
TOPSIS	Technique for Order Preference by Similarity to Ideal Solution

Abstract

From the last few decades there has been increasing demand of compact, integrated and small size products by a non-traditional process for accurate and cost-effective measurement of material properties. These are needed for machining of tools and product design, the development of micro size components, the growing needs for micro-feature generation. Micro-manufacturing processes have good machining performance specifications. Machining performance specifications of concern include minimum feature size, tolerance, surface finish, and material removal rate (MRR). These made the micro wire EDM an important manufacturing process to meet the demands. Micro Wire electrical discharge machining (WEDM) technology has been widely used in production, aerospace/aircraft, medical and virtually all areas of conductive material machining. Material properties such as light weight, high strength and corrosion resistance etc. makes the Aluminum (Al) as a demanding material in the aerospace industry. Aluminum has high coefficient of linear expansion which should be taken in to account at the design state to compensate differences in expansion. Hence there is a need to model for the residual stress before machining the aluminum work piece. This project presents the machining of the aerospace material (Al) using wire EDM with in micro size. The objective of this project is to investigate the performance of micro wire EDM machining of Al material. WEDM is extensively used in machining of conductive materials when accuracy and tight tolerance is important. Simple and easily understandable model for an axisymmetric 2D model for wire electric discharge machining (WEDM) has been developed using the finite element method (FEM). Correctness of the present FEA modeling method has been checked by comparing the present thermal modeling with the previously developed thermal model of INCONEL718 material. The observation have been influenced on various characteristics namely, material

removal rate (MRR) and residual stress. Comparison was done between the theoretical MRR and the experimental results. Design was based on L9 orthogonal array that was taken by Taguchi design of experiment (DOE) approach with three-level, three factors Experiments have been conducted for each experimental run. Three principal component analysis (PCA) based optimization technique have been performed and each optimization results were discussed. It is found that among the three PCA-based approaches i.e. weighted principal component analysis (WPCA), Grey relational analysis (GRA) combined with PCA, and PCA based TOPSIS method. PCA based TOPSIS method results in the best optimization performance in micro WEDM process. Effect of different process parameters (voltage, current, pulse on time) on temperature distribution has also been analyzed from the thermal model of Aluminum work piece.

Keywords: Aluminum**,** Micro WEDM, ANSYS, Modeling, MRR, Residual stress, optimization, WPCA, TOPSIS, Grey relational analysis.

Contents

List of figure

contents

List of table

Contents

CHAPTER 1

1.1 Introduction

Aluminum is a metal having low density hence it has ability to resist corrosion due to passivation. The various Structural components from the aluminum metal are widely used in aerospace industry and other areas of transportation and structural materials. For fulfilling the demands of micro-parts machining various newly developed machining methods has been introduced. Micro-wire electrical discharge machining (μWEDM) is one of them. It has the capabilities to machine micro-parts by micro-wire tool of diameter 20–50 μm and micro-energy pulse generator (1–10 μJ per pulse). Having the advantages of non-contact machining, high efficiency and low cost, micro-WEDM is an excellent process for micro-machining [1].

The material removal protocols for both EDM and WEDM are identical but the functional characteristics are different. Mainly, WEDM requires a thin wire for continuously feeding through the work piece by a microprocessor based control system which supports the various complex parts such as shapes are machined with better accuracy [33]. Due to such advantages the various kinds of micro shaped holes, micro gears, complex micro parts and dies etc. can be machined with a better performance by μWEDM process than other machining process [2]. According to the requirements of the product for industrial use the development of the μWEDM machine has been done with the same principle as that of EDM. The Various categories of EDM process is shown in Fig.1.1.

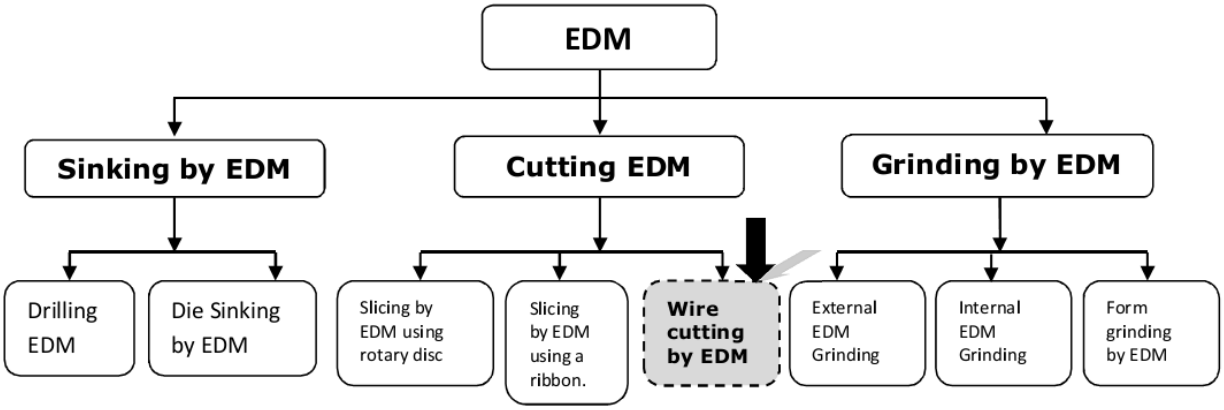

Fig. 1.1 Types of EDM process [3]

Wire electrical discharge machining (WEDM) also known as wire-cut EDM. In this process a thin single brass or copper coated electrode is fed through the work piece which is immersed in the dielectric fluid, mainly deionized water is used as a di electric fluid. The wire-cut types of machines were used in the sixtieth century for the resolution of making tools and dies by hardened steel. The earliest numerical controlled (NC) machines were renovations of punched-tape vertical milling machines. The first commercially available NC machine built as a wire-cut EDM machine was manufactured in the USSR in 1967 [40].

1.2 Principle of wire electrical discharge machining

The Sparking mechanism of wire EDM is same as that of the vertical EDM process. In case of wire EDM, the electro conductive materials are machined with a series of electrical sparks which mainly produced between the electrode and work piece. Under this wire EDM process, high frequency pulses are discharged from the wire to the work piece with a very small spark gap. The insulated dielectric fluid is act as medium for passing of spark current from electrode to work

piece. Typically the gap between wire and work piece for wire EDM varies from 0.025 to 0.05 mm and this gap is constantly monitored by a computer controlled system.

Now a day the numerical control is mainly produced according to the customer requirement for machining. The various parameters such as cutting speeds, machine coordinates, Programs graphics and other relevant information used for this computer control system are displayed in colour monitor as in Fig.1.2. The numerical control offers the capabilities of scaling, mirror imaging, rotation, axis exchange and assist programs which enables user to produce an entire operation from a single program without the need change the main program.

Fig 1.2 Computer numerical system

In the recent years many researchers have attempted to find out the performance characteristics such as material removal rate (MRR), surface roughness (SR) etc. There are many other inter dependence responses to MRR (kerf width, cutting speed) which needs to be optimized for improving performance characteristics of μWEDM process which has been challenging task for the research fraternity. Because of the small size of the micro-part, its dimension accuracy becomes more important in micro-part manufacture. In WEDM, the corner errors and kerf variations mainly caused by the wire tool deflection and vibration in the discharge gap are the main factors to influence the machining accuracy. The kerf variations influencing the dimension accuracy of the micro-parts are more important in micro-WEDM.

CHAPTER 2

Literature review

Dauw et al. [2] highlighted the WEDM applications in many areas such as; machining of various materials used in modern tooling applications, advanced ceramic materials, modern composite materials. They also touched various research opportunities available of WEDM.

Joshi and Pandey have reported the thermo-physical model of die sinking EDM using Finite Element Method (FEM). Modeling had done for material removal rate (MRR), shape of crater cavity. The analysis had been done based on more realistic assumption such as Gaussian distribution of heat flux, spark radius based on more realistic model based on discharge current, discharge duration, discharge voltage and duty cycle on the process performance. They compared the reported analytical model with the presently developed model and it was found that present developed model predicts closer result to the experimental results [3].

Hewidy et.al [4] highlighted the development of mathematical models for comparing the interrelationships of various WEDM machining parameters in Inconel 601 material such as; peak current, duty cycle, wire tension and water pressure on the volumetric metal removal rate (VMRR), wear ratio (WR) and surface roughness (SR). This work had been established based on the response surface methodology (RSM) approach. It was reported that analysis of the response parameters using RSM technique has the advantage of explaining the effect of each working parameter on the value of the resultant response parameter. The volumetric metal removal rate generally increases with the increase of the peak current value and water pressure. This trend is

valid up to the generation of arcing, after certain limit, the increase of the peak current leads to the decrease of VMRR.

Scott et al. [5, 34, 35, 36] used a factorial design demanding a number of experiments to determine the most promising combination of the WEDM parameter. They found that the discharge current, pulse duration and pulse frequency are the significant factors that affects the MRR and SF, while the wire speed, wire tension and dielectric flow rate effect less in the machining performance.

Liao et al. [6, 37] anticipated an approach to determine the parameter settings based on the Taguchi quality design method and the analysis of variance. The results showed that the MRR and SF can be easily influenced by the table feed rate and pulse on-time, which can also be used to control the discharging frequency for the prevention of wire breakage.

Padding and Wang[7] developed the modeling techniques using the response surface methodology and artificial neural network technology to predict the process performance such as CR, SF and surface waviness within a reasonable large range of input factor levels.

Somashekhar *et al* [8]. optimized the micro WEDM Simulated Annealing (SA) scheme. The important parameters of Material Removal Rate (MRR), overcut and surface roughness had been considered in the study of single pass μWEDM machining of aluminum. This system model is employed to maximize the material removal rate and minimize the surface roughness and overcut using Simulated Annealing (SA) scheme. Series of experiments has been conducted with three levels full factorial experimentation using Design of Experiments with factors gap voltage, capacitance and feed rate. Capacitance was identified as the most significant factor that affects

the performance. They showed that simulated annealing approach can systematically search the process parameters for obtaining optimum process parameters.

Mu-Tian Yan and Hsing-Tsung Chien developed the pulse discriminating and control system in micro WEDM. The pulse discriminating and control system had been classified in to four major gap states as open circuit, normal spark, arc discharge and short circuit based on the characteristics of gap voltage waveform. It was found that a long pulse interval results in an increase of the short ratio under a constant feed rate machining condition. They proposed the control strategy by regulating the pulse interval of each spark in real-time according to the identified gap states. The developed pulse discriminates and control system that can significantly reduce the arc discharge and short sparking frequency as well as achieve stable machining under the condition where the instability of machining operation is prone to occur. They concluded that proportion of short circuits (short ratio) and the sparking frequency can be employed to monitor and evaluate the gap condition. According to the classification of discharge pulses, a pulse interval control strategy had been proposed to improve the abnormal machining condition [9].

A. Mohammadi[10, 41, 42] *et al.* has found out how the effects of power, time-off, voltage, servo, wire speed, wire tension, and rotational speed (factors) on the MRR (response) in WEDM. An L18 Taguchi standard orthogonal array was chosen for the design of experiments. Analyses of variance (ANOVA) as well as regression analysis were performed on experimental data. The signal-to-noise (S/N) ratio analysis was employed to find the optimal condition. A good result cannot be gained through statistical analyses of experimental data unless the experimentation is provided with a carefully conducted design of experiments (DOE).Taguchi standard orthogonal arrays are nowadays predominant Spindle in five-axis WEDM machine

T. A. Spedding and Z. Q. Wang [11] attempted at optimization of the process parametric combinations by modeling the process using artificial neural networks (ANN) and characterizes the WEDMed surface through time series techniques. A feed forward back propagation neural network based on a central composite rotatable experimental design was developed to model the machining process. Optimal parametric combinations are selected for the process. Pulse width, time between two pulses, wire mechanical tension were taken as input factors and cutting speed, work piece surface roughness and waviness were selected as the process outputs. It was found that the cutting speed of the process had an upper limit and reduced rapidly with a decrease of required surface roughness value .

S.K Gauri and S Chakraborty [12, 13] highlighted the computational requirements for these four standardized multi-response optimization methods (e.g., GRA, MRSN ratio, WSN ratio, and VIKOR methods). Two sets of experimental data on WEDM processes are analyzed using these standardized multi-response optimization methods, and their relative performances were then compared. The results show that no method can lead to better optimization than the WSN ratio method. They applied weighted principal component (WPC) method for optimizing the WEDM process and observed that the WPC method results in better overall optimization performance than the MRSN ratio method.

FU [29,43] *et al*. Investigated optimization problem of the cutting parameters in high-speed milling on NAK80 mold steel. Experiment was done based on Taguchi technique. They had tried to establish a correlation among spindle speed, feed per tooth and depth of cut to the three directions. It was showed that grey relational analysis coupled with principal component analysis can effectively obtain the optimal combination of cutting parameters.

Tong [30] *et al*. applied PCA combined with TOPSIS for optimizing multi objective problems of the chemical-mechanical polishing of copper (Cu-CMP) thin films. They explained the PCA with TOPSIS optimization technique taking a case study. The proposed procedure resolved the multi-response problems in a dynamic system with some modification.

Liao [31] compared PCA method with WPCA optimization technique two overcome two shortcomings and three case studies were done to illustrate and compare in the application of WPC method. The result showed that the WPC method offers significant improvements in quality.

Das and Joshi [32] model the spark erosion rate in micro wire EDM. a ample mathematical model was developed to include plasma features, moving heat source characteristics, multi-spark phenomenon, and wire vibrational effect to predict the cathode erosion rate for a single and multi-spark in micro-WEDM. The erosion rate estimated by the model showed that it is independent of the wire velocity.

CHAPTER 3

Modeling of micro WEDM

3.1 Introduction

In the present work thermal modeling has been done for wire EDM, and the material removal rete was estimated using the simplified equation. A 2-D rectangular domain of the work piece having size $100\mu m \times 20\mu m$ is taken for the analysis. Three different graphs have been drawn by increasing each control parameter and by fixing the other two. Temperature distribution Vs distance graph on the upper edge and the left vertical edge of the rectangular domain where depth (Y) =0 and radius (r) =0 has been plotted. The theoretically calculated MRR values drawn from the modeling were compared with the experimental results. Modeling has also been done for residual stress developed after restricted the cooling of the work piece up to t_{off} time which is fixed at 100µm. This has been completed by coupled thermal- structural analysis using ANSYS13. Displacement of the work piece due to residual stress is also shown and their values were recorded.

ANSYS13 is a strong tool for prediction and simulation a of the physical problems such as solid modeling, fluid flow problems, heat flow model etc. This is mainly important in aerospace component design, which requires knowledge in thermal, aerodynamic, structural and electronics field to solve the problem.

3.2 Modeling process of micro Wire EDM using ANSYS by finite element method (FEM)

Finite element analysis (FEA) method is being broadly used in the industries to simulate structures and the loads that act on them. This method allows users to foresee how a product will

respond in real-time situations before they are implemented in to that product. As a result, they are able to modify their designs and materials by a limited number of sample stages. This saves money both in the cost of materials and the time taken for real time testing. The process of solving systems of equations is described as below.

3.2.1 Discretize the Domain

The first step involves breaking up the domain of the problem into subsections called Elements. These elements can take on many different shapes such as triangles or quadrilaterals. They are characterized by a certain number of nodes which define the geometry of each of the element. Fig. 3.1 provides an illustration of how this procedure works. Here, a square control volume is broken up into four quadrilateral elements each with four nodes associated with them.

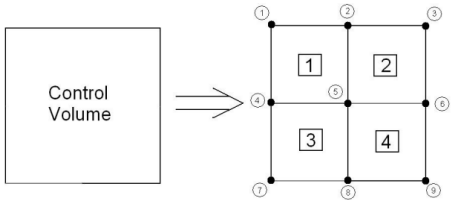

Fig.3.1 Discretized control volume

3.2.2 Develop Shape Functions

After the domain has been discretized, approximate solutions are assumed over each of the elements created. These solutions are called shape functions, or interpolation functions. They are generally quadratic functions as these are easily differentiated. In Fig. 3.2, a 1-D linear element is shown. Let us assume a solution for the temperature across that element can be approximated by the following linear function (1):

Fig.3.2 1-D linear element

$$T=\alpha_1+\alpha_2 x \quad (1)$$

$where\ \alpha_1$ and α_2 are constants which will be solved. Substituting the values at nodes 1 and 2 into Equation 1 provides:

$$T_1=\alpha_1+\alpha_2 x_1 \tag{2}$$

$$T_2=\alpha_1+\alpha_2 x_2 \tag{3}$$

By solving Eq.2 and Eq3 α_1 and α_2 are found as, then substituting these values in Eq.1, the final Equation becomes

$$T=T_1\left[\frac{x_2-x}{x_2-x_1}\right]+T_2\left[\frac{x-x_1}{x_2-x_1}\right]=N_1T_1+N_2T_2 \tag{4}$$

Differentiating Equation 1 provides the temperature gradient across the element.

$$\frac{dT}{dx}=\frac{dN_1}{dx}T_1+\frac{dN_2}{dx}T_2=-\frac{1}{x_2-x_1}T_1+\frac{1}{x_2-x_1}T_2 \tag{5}$$

Eq. 4 and Eq.5 define the approximated temperature and temperature gradient across the entire element. For a system of many elements and nodes, this process is done iteratively, with shape functions being applied to each element in the system. From here a system of matrices is developed to put the entire system of equations into a form shown in Eq. 6.

$$[K]\{T\}=\{f\} \tag{6}$$

Where $[K]$, the collection of the entire coefficient, $\{T\}$ is the nodal temperatures and temperature gradients and $\{f\}$ is the collection of known values of the system. This system of equations is then solved and the nodal values for the dependent variables in $\{T\}$ are found.

3.3 Thermal modeling of EDM to micro Wire EDM

The primary mechanism of material removal in EDM process is the thermal heating of work surface due to intense heat generated by the spark, which raises the temperature of the electrodes (tool, work) beyond their melting point, sometimes even the boiling point. For the

thermal analysis of the process, conduction is thus considered as the primary mode of heat transfer between the ions of plasma and the molecules of work/tool [14, 15, 16, and 17].

3.3.1 Assumptions

The following assumptions have been considered in the thermal modeling procedure [3]

1. The work piece is considered as a semi-infinite body since the volume of the removed materials is much smaller than the volume of the work piece.
2. Bilateral thermal effects of successive sparks are neglected.
3. The effects of sparking gap on discharged characteristics are supposed to be neglected.
4. Crater formed on the work piece due to each discharge is assumed as circular parabolic shape.
5. Flushing efficiency is considered to be 100%. That means there is no recast layer formation on the machined surface.
6. Work piece and tool materials are homogeneous and isotropic in nature.
7. Joule heating and cross-vibration effects of the moving wire are neglected.
8. The work piece is free from any type of stress before process.

3.3.2 Thermal Modeling

A cylindrical portion of work pieces chosen for the model analysis, Transnet analysis of uniform heat flux with axis-symmetric model is assumed. Present model analysis is the idealized case where work piece is being heated by a Gaussian type of heat source. The mode of heat transfer is due to conduction and convection only.

3.3.3 Governing Equation

The governing equation of heat conduction in two dimensional bodies is given in Eq.7:

$$\frac{1}{\propto}\frac{\partial T}{\partial t}=\frac{\partial 2y}{\partial r^2}+\frac{1}{r}\frac{\partial T}{\partial r}+\frac{\partial 2y}{\partial z^2} \quad (7)$$

Where ∝(thermal diffusivity)=k/ρc; ρ is the density of the work piece; *c* is the specific heat of the work piece; T is the temperature of the work piece; r and z are the co-ordinate axes; t is the time.

3.3.4 Initial condition

Initially temperature of the work piece is assumed to room temperature. i.e at time (t=0), temperature (T_0) is 298K.

3.3.5 Boundary conditions

A rectangular 2D model (100μm×20μm) is developed by ANSYS13.0 and it is adequately meshed with optimum mesh area size of 1μm. Heat flux is used to simulate spark energy in the region of the plasma radius (R), the region larger than R is applied convection boundary condition on the top surface and the other three surfaces are insulated i.e. $\frac{\partial T}{\partial n}$=0. Percentage of Heat input is denoted by q and the convection heat transfer is expressed as $h_c(T-T_0)$. Fig.3.3 shows the Schematic representation of the domain considered for the numerical model and Fig.3.4 shows the Boundary conditions of wire EDM.

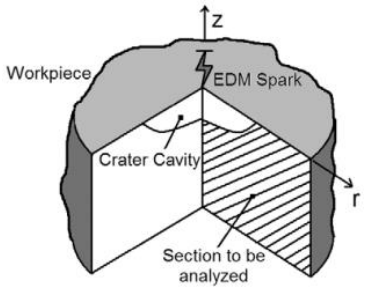

Fig.3.3 Schematic representation of the domain considered for the numerical model [3]

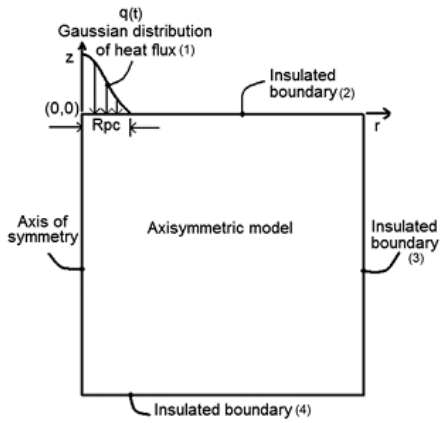

Fig.3.4. Boundary conditions of wire EDM

- In the Fig.8, Boundary 2 and 3 are considered to be insulated. i.e $\frac{dT}{dn}$=0, where n is the normal direction of boundary layer2 and 3.
- Heating is axy-symmetric to the axis of the spark, so heat flowing from the counter part of the domain is equal to the heat flowing out of the counterpart. Therefore no heat gain or loss from the counter part of the surface domain. i.e. $\frac{dT}{dr}$=0 at r=0.
- On the upper layer, at boundary1, spark is directly contacted with the surface. Hence heat flux boundary condition is applied.
- At boundary 2, heat transfer takes place due to convection only. So convective boundary condition is applied at different conditions which shown in eq.8;

$$\begin{cases} K\left(\frac{dT}{dz}\right)=h_c(T-T_0) & \text{if } r>R \\ =q_w & \text{if } r=R \\ =0 & \text{during off time} \end{cases} \quad (8)$$

3.3.6 Heat input

Important factors which contribute to the accurate calculation of the MRR in single spark EDM model include the amount of heat input, radius of plasma spark and the thermo-physical properties of material [18]. In this present work, the Gaussian distribution of heat flux input has been used to approximate the heat from the plasma. The heat flux calculation equation is derived [3] as given in Eq.9.

$$q_W(r) = \frac{4.45 R_w V_C I_C}{\pi R^2} \exp\left\{-4.5\left(\frac{r}{R}\right)^2\right\}, \quad (9)$$

Where r is the radial distance from axis of the spark, R is the spark radius, Vc is the critical voltage and Ic is the critical current.

3.3.7 Material properties

The material properties have greater role in the distribution of temperature inside the work piece and MRR. Material properties are also important factor to generate residual stress after machining.

3.3.8 Spark Radius

Spark radius is an important factor in the thermal modeling of EDM process. In actual practice, it is very difficult to measure spark radius due to very short pulse duration of the order of few microseconds [19]. Predicted by Pandey and Jilani [20] about spark radius equation based on boiling point temperature is notable. Ikai and Hashiguchi [27] have derived a semi-empirical equation of spark radius (Eq.10) termed as ``equivalent heat input radius" which is a function of discharge current, I (A) and discharge on-time, ton (µs). It is more realistic when compared with the other approaches.

R_{pc}= (2.04e-3)$I^{0.43} t_{on}^{0.44}$ (µm) (10)

According to Donald et al [22], the Spark Theory on a wire EDM is basically the same as that of the vertical EDM process. In this process many sparks can be observed at one time. This is because actual discharges occurs more than one hundred thousand times per second, with discharge sparks lasting in the range of 1/1,000,000 of a second or less. The volume of metal removed during this short period of spark discharge depends on the desired cutting speed and the surface finish required.

3.4 Finite Element Analysis Procedure

The general finite element modeling procedure consists of the following steps [38].

i. Preprocessing

- definition of Element type
- Material properties definition
- Model generation

ii. Solution

- Defining initial condition
- Applying boundary condition
- Applying load
- Solving for results

iii. post processing

- Reading result file
- Viewing results

3.4.1 *Preprocessing*

3.4.1.1 Definition of Element type

Defining element type plays is the major factor to achieve accuracy of the outcome and reduction of solution time for finite element analysis. In the present analysis element type chosen is PLANE55. PLANE55 is used as a plane, ax symmetric thermal solid element with a 2-D thermal conduction capability. The element abstains four nodes with a single degree of freedom (temperature) at each node.

3.4.1.2 Material properties

Aluminum is the most common structural material used in the aerospace components. It has nonlinear material properties, viz. temperature dependent thermal conductivity. For the model analysis Al has been chosen and for conformation of thermal modeling INCONEL718 material was chosen.

3.4.1.3 Finite Element modeling of the work piece

A rectangular work piece of size 100µm× 20µm was generated by picking key points on the ANSYS work bench. The optimum mesh size is taken as 1µm for the analysis. After the modeling work is expanded for Micro Wire EDM with the different parameter, ANSYS Parametric Design is used to build the single spark EDM model. Two-dimensional view of the meshed model with element size of 20µm is shown in Fig.3.5.

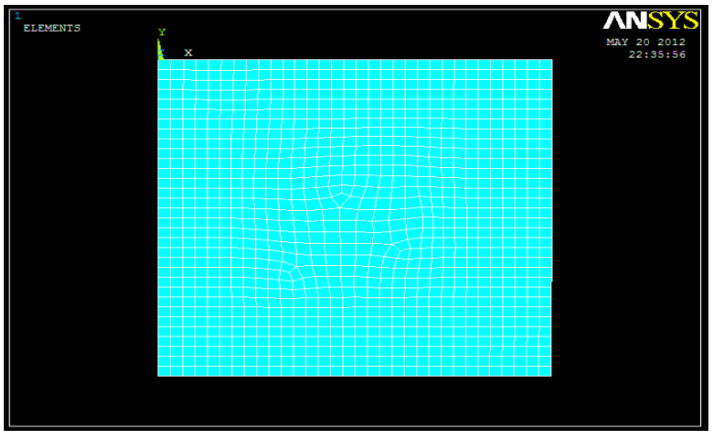

Fig.3.5 Two-dimensional view of the meshed model with element size of 10µm

3.4.2 Solution

3.4.2.1 Application of Thermal Loads

Gaussian heat flux was applied on the top surface of the upper layer elements present in the finely meshed zone, which were within the vicinity of the spark radius. The convective load is applied on the upper surface layer except spark region.

3.4.3 Post processing

In the post processing stage, the temperature contour plots, time temperature plot of nodes along the depth and radius can be seen.

3.5 Modeling of MRR of µ wire EDM

Actual material removal rate during WEDM process is administered by many factors such as ignition delays, high frequency of sparks, flushing efficiency, and phase change of electrodes, dielectric medium, and random behavior of debris particles etc. The nodes which are having temperature more than melting point temperature are removed from the complete work domain. At the end of pulse on time a crater cavity is formed. The present analysis is for single spark problem. Total crater volume is divided in to small cylindrical disc shape. The volume of

each disc is calculated and then adding all disc volume, the crater volume is found out. 2-D view of One fourth of the models for calculation of crater volume is shown in Fig. 3.6.

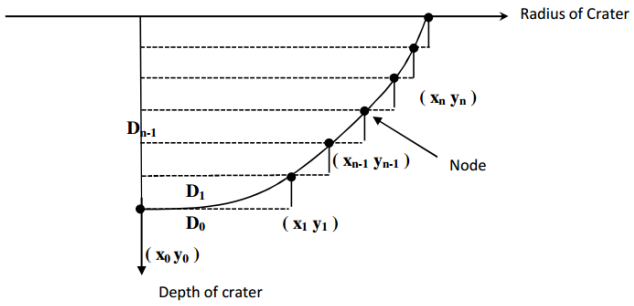

Fig.3.6 Calculation of crater Volume

$$D_i = \pi \left(\frac{X_i + X_{i+1}}{2}\right)^2 (y_i + y_{i+1}) \quad (11)$$

Where D_i Is the volume of a disc, where x and y are the coordinates of nodes and n is the number of nodes.

It is very difficult to incorporate all the factors into the numerical process models. As a result, in the present work, ideal MRR was computed for chosen process conditions considering that all sparks are equally effective.

The MRR (mm^3/min) of single spark is computed by

$$\text{MRR} = \frac{60 \times C_v}{t_{on} + t_{off}} \quad (12)$$

Where C_{vt} (µm) is the volume of crater per unit discharge and t_{off} is discharge off time.

3.5.1 MRR calculation for multi- discharge

For the multi discharge analysis [24]

$$\text{No. of pulses} = \frac{T_{machining}}{t_{on} + t_{off}} \quad (13)$$

$MRR_{multi-discharge}$ = no. of pulses × $MRR_{single-discharge}$ (14)

3.6 Measuring residual stress caused by Wire EDM

Residual stresses are those stress which acts inside the body by itself when the thermal or mechanical loads are removed. These forces come in to existence, when there is a sharp temperature gradient due to re-solidification of material on the work piece, causes thermal contraction. Plastic deformation of material results in the development of residual stress [25]. Residual stress trend perhaps changed by the metallurgical alteration relating volumetric changes, as it is well known that the martensitic transformation from austenite with a concurrent increase in specific volume of about 3% [26].

3.6.1 Thermo-mechanical analysis

The global coupled thermo-mechanical model for the Micro Wire EDM simulation assumes a two-dimensional Gaussian heat flux distribution in a cylindrical volume, which moves along the cutting path. By applying the thermal and mechanical boundary conditions a coupled thermo-mechanical analysis may be executed and temperature distributions and residual stresses can be calculated. An overview of the step by step procedure to predict the distribution of temperature and residual stress is in the flow chart shown in Fig. 3.7. An over view of the numerical procedure as described in the flow chart shown in Fig.3.8. In this model temperature dependent thermal and mechanical properties of materials are introduced.

3.6.2 Modeling steps for residual stress (coupled thermal –structural analysis)

- ✓ Create a rectangular model of size 100μm×20μm. Element type PLANE55 was chosen which is for 4 nodded quadrilateral thermal solid element.

- ✓ Defining material properties and optimum mesh size of 1µm was taken. Temperature dependent thermal conductivity, density, heat capacity.
- ✓ Apply thermal boundary conditions and initial temperature was set to 298K.
- ✓ Solve by current load step.
- ✓ Switch the loading title from thermal to structural. The solution of the thermal analysis was applied as a load in for the structural analysis.
- ✓ Applying boundary conditions for structural analysis.
- ✓ Read and plot results.
- ✓ Finish.

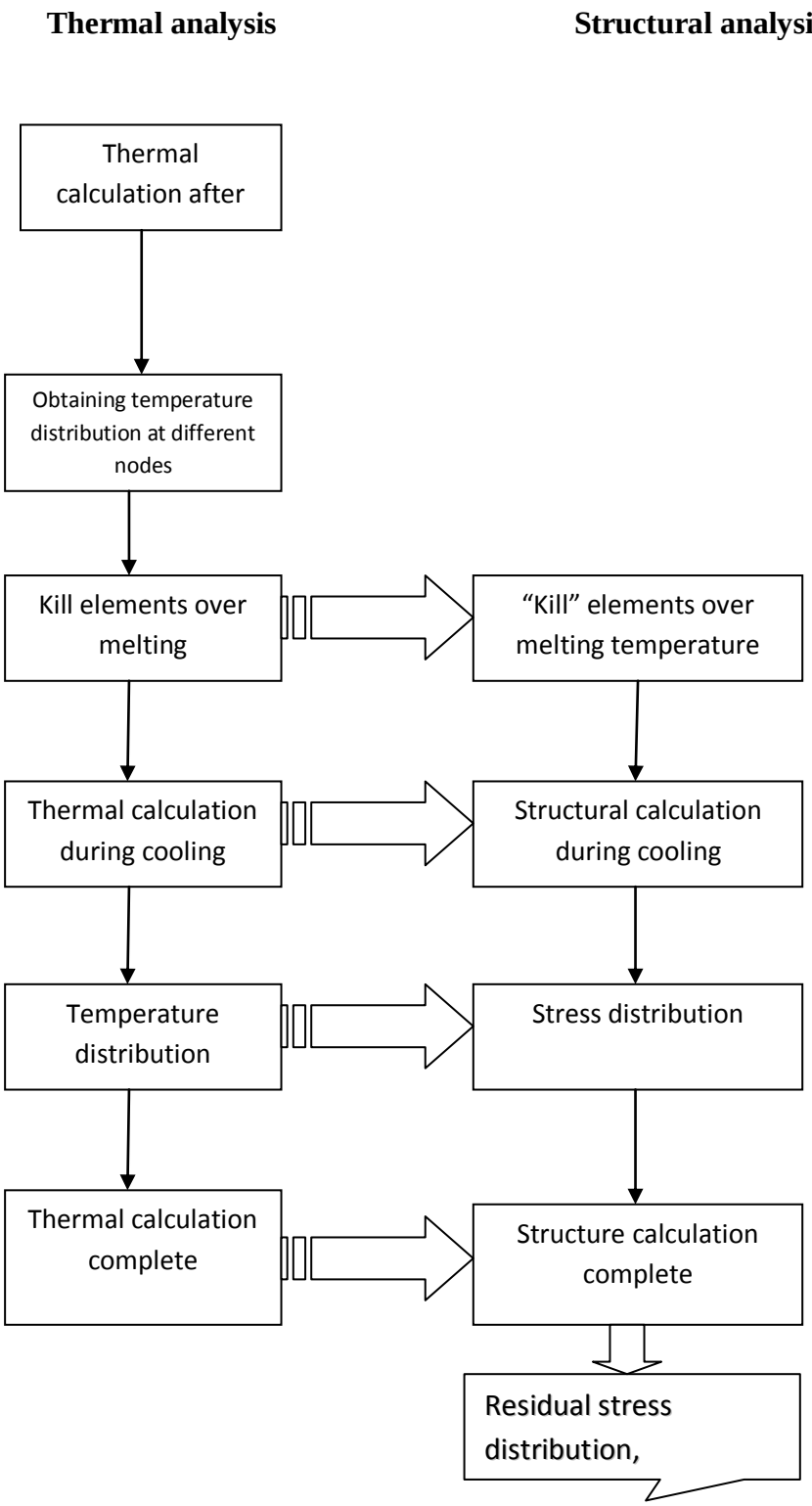

Fig. 3.7 Flow chart of procedure for thermal modeling and residual stress

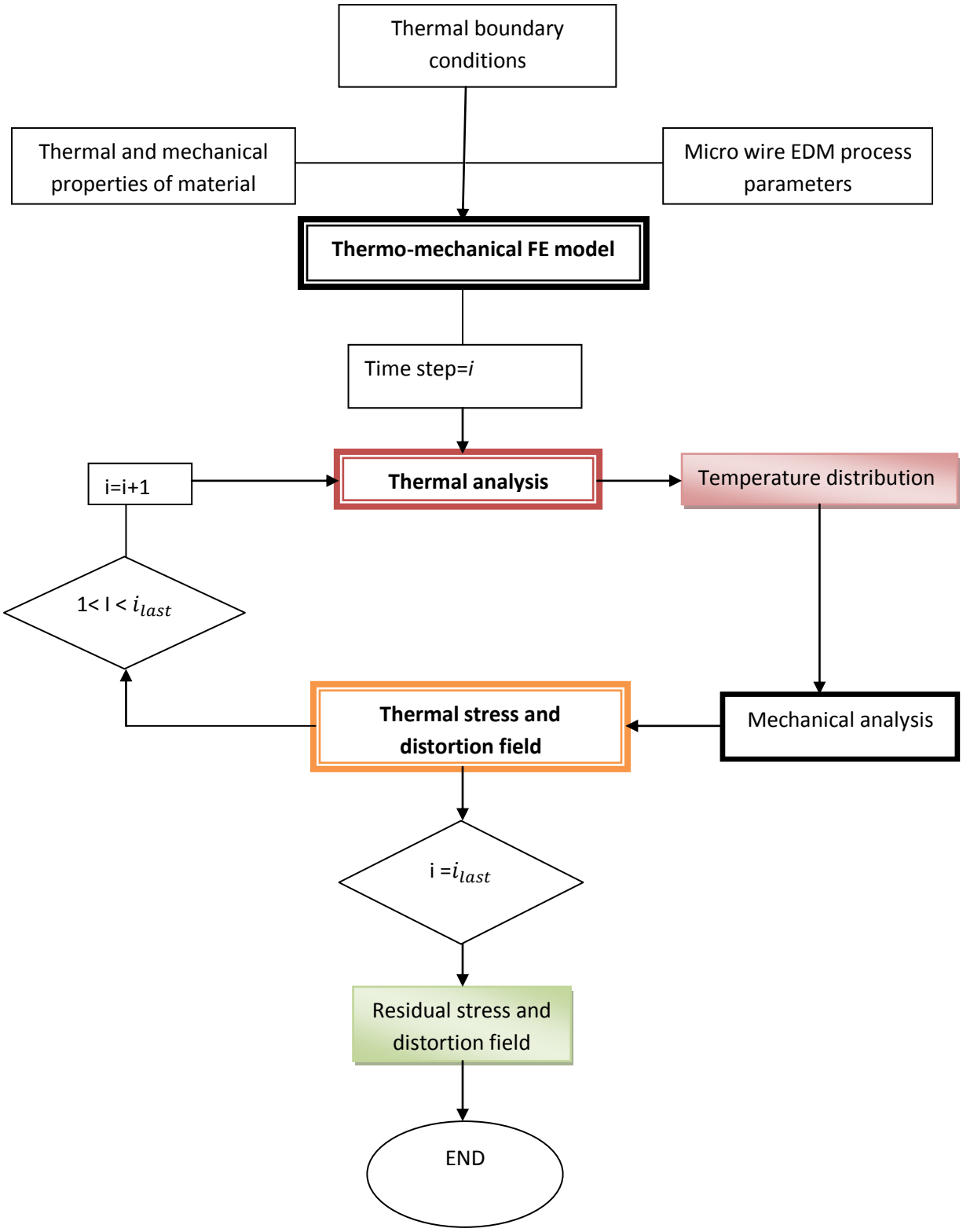

Fig.3.8 Over view of numerical procedure to find out residual stress

CHAPTER 4

Optimization Technique

4.1 Multi- objective Optimization

The WEDM process, which is a combination of electrodynamics, electromagnetic, thermal dynamic and hydrodynamic actions, exhibits a complex and stochastic nature. Its performance, in terms of machining productivity, accuracy is affected by many factors. Wire EDM manufacturers and users always want to achieve higher machining productivity with a desired accuracy and surface finish. Performance of the WEDM process, however, is affected by many factors (work piece material, wire, dielectric medium, adjustable parameters, etc.) and a single parameter change will influence the process in a complex way.

In micro wire EDM processes there are three dependent responses i.e. Material removal rate, kerf width, cutting speed are needed to be optimized simultaneously. Hence three different multi-objective optimization techniques have been introduced. To element inter dependency of among responses during optimization, principal component analysis (PCA) based optimization techniques are applied.

4.1.1 Weighted principal component Analysis

Taguchi is a robust design method only applied to optimize a single-response problem. Researchers' show that the multi-response problem is quiets an issue with the Taguchi method. Some researchers have tried to optimize WEDM operations using MRSN ratio & constraint optimization methods [39].

Principal component analysis (PCA) is used to explain the variance-covariance structure of a set of variables by linearly combining the original variables. The PCA technique can account for most of the variation of the original p variables via q uncorrelated principal components, where q≤p. In the context of Taguchi is robust design experimentation, let there being m experimental trials, and in each trial, quality losses of a set of p performance characteristics (response variables) are measured. Therefore, (L) m×p will be the experimental data set. Taguchi categorized the performance characteristics (response variables) into three different types, e.g. the smaller-the-better, the larger-the-better and nominal the best. The formulae for computation of quality loss (Lij) for jth response corresponding to ith trial (i=1, 2... m; j=1, 2... p) Are different for different types of response variables, and these are given as follows:

For smaller-the-better,

$$L_{ij}= (\frac{1}{n} * \sum_{k=1}^{n} Y_{ijk}^2) \quad (15)$$

For larger-the-better,

$$L_{ij} = (\frac{1}{n} * \sum_{k=1}^{n} \frac{1}{Y_{ijk}^2}) \quad (16)$$

For nominal-the-best,

$$L_{ij} = (\frac{\mu^2}{\sigma^2}) \quad (17)$$

Where $\mu=\frac{1}{n}\sum_{k=1}^{n} Y_{ijk,}\ \sigma^2 = \frac{1}{n-1}\sum_{k=1}^{n}\left(Y_{ijk} - \mu\right)^2$, n represent the number of repeated experiments, Y_{ijk} is the experimental value of j_{th} response variable in i_{th} trial at k_{th} test and L_{ij} is the computed quality loss for j_{th} response in i_{th} trial.

Through the PCA, the variability in the original p response variables corresponding to ith trial can be explained by the following q uncorrelated linear combinations:

$$\Omega_l^i = a_{1l}L_{i1} + a_{2l}L_{i2} + \ldots\ldots\ldots\ldots\ldots + a_{pl}L_{ip};\ (l = 1,2 \ldots\ldots, q) \quad (18)$$

Further, W_{i1} is called the first principal component; W_{i2} is the second principal component and so on.

The coefficients of the l_{th} component, i.e. $a_{l1}, a_{l2}, \ldots., a_{lp}$, are the elements of the eigenvector corresponding to the l_{th} eigenvalue of the correlation matrix or the covariance matrix of the response variables. The eigenvalues for the q components and the eigenvector corresponding to each eigenvalue can be obtained by subjecting the experimental data set, $(L)_{m\times p}$, to principal component analysis. The option of performing the PCA is available in MINITAB 16 software. The eigenvalue of a principal component gives a fairly good idea about the variance of the original variables that can be explained by the principal component. A larger eigenvalue of a principal component implies that the component's contribution in explaining the overall variation is higher.

The weighted principal component (WPC)-based procedure for optimization of multi-response processes makes use of all the principal components irrespective of the eigenvalues so that the overall variation in all the responses can be completely explained. In this approach, the proportion of overall variation explained by each component is treated as the weight to combine all the principal components in order to form a multi -response performance index (MPI). Then the best combination of the parametric settings can easily be obtained that can optimize the MPI. It may be noted that Liao applied the WPC method.

It may be noted that Liao applied the WPC method Considering computed quality losses, i.e. $(L)_{m\times p}$ as the experimental data. Here it is suggested to compute the signal-to-noise (S/N) ratio, which is the logarithmic transformation of the quality-loss function, for each response in each trial. This is because the logarithmic transformation improves additive of effects of two or more control factors. The WPC method for multi-response optimization can be described in the following five steps:

Step 1: Compute the signal-to-noise (S/N) ratio for each response.

Depending upon the type of the quality characteristic, calculate the quality loss (L_{ij}) of j_{th} response corresponding to i_{th} trial using Eq. (9) or (10) or (11), and then, compute the S/N ratio (η_{ij}) value for j_{th} response corresponding to i_{th} trial using Eq. (12) as shown below

$$\acute{\eta}_{ij}=-10\log_{10}L_{ij} \tag{19}$$

Where $\acute{\eta}_{ij}$ is the signal-to-noise (S/N) ratio.

Step 2: Transform the S/N ratio values for each response into (0, 1) interval.

Normalizing the S/N ratios of each response reduces the variability among those values for different responses. $\acute{\eta}_{ij}$ is transformed into Yij ($0\leq Yij\leq 1$) using the following equation;

$$Y_{ij}=\frac{\acute{\eta}_{ij}-\acute{\eta}_j^{min}}{\acute{\eta}_j^{max}-\acute{\eta}_j^{min}} \tag{20}$$

Where, Y_{ij}= normalized S/N ratio value for j_{th} response at i_{th} trial.

Step 3: Perform the PCA on the computed data, $(Yij)_{m\times p}$ and obtain the principal components.

Subject the data set, $(Yij)_{m\times p}$, to principal component analysis and obtain the eigenvalues of the q principal components and the eigenvector corresponding to each eigenvalue. Then, similar to Eq. (12), obtain the q principal components corresponding to a trial (i) as follows:

$$Z_l^i = a_{1l}L_{i1} + a_{2l}L_{i2} + \ldots\ldots\ldots\ldots\ldots + a_{pl}L_{ip};\ (l = 1,2 \ldots \ldots, q) \quad (21)$$

Step 4: Compute the multi-response performance index (MPI) corresponding to each trial

The multi-response performance index (MPI) is essentially the weighted sum of all the principal components. The MPI value for i_{th} trial, therefore, can be computed using the following equation:

$$MPI^i = \sum_{l=1}^{q} W_l\, Z_l^i \quad (22)$$

Where, W_l is the proportion of overall variance of the responses explained by lth principal component, Z_l^i is the computed value of lth principal component corresponding to ith trial and It may be noted that since all the principal components are independent of each other, A larger value of MPI is considered the better quality.

Step 5: Determine the optimal factor/level combination and confirm

Carry out the analysis of variance (ANOVA) on MPI values to identify the significant factors (process parameters). Compute level averages, i.e. average MPI values at different levels of the control factors. A larger MPI value implies better process performance and so selects the level averages of the influencing factors that lead to higher value for MPI.

4.1.2 Grey relational analysis coupled with principal component analysis

Step1. Grey relational analysis

Grey relation is the certainty of association among things or uncertainty between system factors and the main behavioral factors. It measures the degree of proximity according to similarity or difference among the development situations of factors. The grey relational analysis is used to convert the multi responses which need to be optimized to a single objective. The flow chart for purpose of grey relational analysis is shown Fig.4.1.

Fig.4.1 Purpose of grey relational analysis

Step2. Data normalization

In the grey relational analysis, data normalization is the first step where in a data sequence, the original data requires normalization to get a comparable sequence because of different scope and dimension. In a linear normalization the values of all the responses lie in between 0 to 1 is also called as grey relational generation.

The "smaller-the-better "is a characteristic of the original sequence and it should be normalized as follows:

$$x_i^*(\mathrm{k})=\frac{\max x_i^{(0)}(\mathrm{k})-x_i^{(0)}(\mathrm{k})}{max\, x_i^{(0)}(\mathrm{k})-\min x_i^{(0)}(\mathrm{k})} \tag{23}$$

i=1, 2, 3…….m; k=1, 2, 3……n;

Where $x_i^{(0)}$(k) is the original sequence of the MRR, kerf width and cutting speed; x_i^*(k) is the comparable sequence after data normalization; *m* is the number of experiments; *n* is the number of response variables; $max\ x_i^{(0)}$(k), $min\ x_i^{(0)}$(k) are respectively the largest value and smallest value of $x_i^{(0)}$(k). Presently m=9,n=3 are taken.

Step3. Grey relational coefficient and grey relational grade

Obtain the grey relational coefficients based on normalized principal component scores. The grey relational coefficient of l_{th} normalized PCS in i_{th} trial (γ_{il}) is calculated as follows:

$$\gamma_{il}=\frac{\Delta_l^{min}+\xi\Delta_l^{max}}{\Delta_{il}+\xi\Delta_l^{max}} \quad (24)$$

Where $\Delta_{il}= \left| 1 - x_i^*(k) \right|$, Δ_l^{min}=min{ $\Delta_{1l}, \Delta_{2l}, \Delta_{3l} \dots\dots\dots\dots \Delta_{ml}$}

and Δ_l^{max}=max{ $\Delta_{1l}, \Delta_{2l}, \Delta_{3l} \dots\dots\dots\dots \Delta_{ml}$}, and ξ= distinguishing co-efficient. Its value lies in between 0 and1. Its value is usually set as 0.5.Then the Grey relational grade (OQPI) value can be calculated by the following formula;

$$OQPI_l=\sum_{l=1}^{p} w_l\ \gamma il \quad (25)$$

Step4. Optimal factor levels can be found out by the- higher- the –better factor effects.

4.1.3 PCA-Based TOPSIS Method

In PCA-Based TOPSIS Method single process performance index (PPI) is called the overall performance index (OPI). The OPI is essentially the measure of relative closeness to the ideal solution obtained in TOPSIS method. The PCA-based TOPSIS method can be applied based on following 12 steps:

Step 1: Calculate the S/N ratio for each response variable corresponding to each trial.

Step 2: Normalize the S/N ratio of each response variable using the following equation:

$$Y_{ij}=\frac{SN_{ij}-\overline{SN}}{SN_{SN_j}} \tag{26}$$

Where SN_{ij} denotes the S/N ratio of j_{th} response variable in i_{th} trial, $\overline{SN}$ and SN_{SN_j} represents the mean and standard deviation of the S/N ratio for j_{th} response respectively.

Step 3: Conduct PCA on the normalized S/N ratios of the response variables, and obtain the Eigen values, eigenvectors, and the proportion of variation explained by different principal components.

Step 4: Determine the number of principal components retained. The number of principal components retained should account for almost 100% of the variation in the original variables.

Step 5: Establish the variation mode charts and determine the optimization direction of the selected principal components.

Step 6: Establish an alternative performance matrix, where m trials are the possible alternatives and the selected principal components are the performance measures. The l_{th} performance measure corresponding to i_{th} trial (D_{il}) can be computed as follows:

$$R_{il}=\frac{D_{il}}{\sqrt{\sum_{i=1}^{m} {D_{il}}^2}} \tag{27}$$

Where R_{il} represents the normalized value of the lth performance measure corresponding to ith trial.

Step 8: Obtain the weighted performance matrix. The weighted performance measure for the lth attribute corresponding to the ith trial (Vil) can be derived as follows:

$$\text{Vil}=\lambda_1 R_{il} \tag{28}$$

Step 9. Determine the ideal and the negative-ideal solutions. The ideal value set, $V^+$and the negative-ideal value set,V^- are determined as follows:

$$V^+ = \{(\max \text{Vil} \mid 1\epsilon \text{ L, or } (\max \text{Vil} \mid 1\epsilon L^{|}),\ i= 1, 2, 3\ldots.m\} = \{V_1^+, V_2^+, V_3^+, \ldots..,V_q^+\} \tag{29}$$

$$V^+ = \{(\max \text{Vil} \mid 1\epsilon \text{ L, or } (\max \text{Vil} \mid 1\epsilon L^{|}),\ i= 1, 2, 3\ldots.m\} = \{V_1^+, V_2^+, V_3^+, \ldots..,V_q^+\} \tag{30}$$

Where

L={1, 2, 3,...., p ⎪ Vil , a larger response is desire}

$L^{|}$ = {1, 2, 3,...., p ⎪ Vil , a smaller response is desire}

Step10. Then separation measures are calculated. The separation of each alternative from the ideal solution (S_i^+) is given by:

$$S_i^+ = \sqrt{\sum_{l=1}^{p} (\text{Vil} - \text{V}_\text{l}^+)^2} \tag{31}$$

The separation of each alternative from the negative-ideal solution (S_i^-) is given as follows:

$$S_i^- = \sqrt{\sum_{l=1}^{p} (\text{Vil} - \text{V}_\text{l}^-)^2} \tag{32}$$

Step11. the relative closeness of various alternatives to the ideal solution is to be calculated. It is considered as the *OPI*. The *OPI* value for the i^{th} trial can be computed as follows:

$$OPI=\frac{s_i^-}{s_i^+ + s_i^-} \quad (33)$$

Step12. The optimal factor level combination is decided by the- higher-the- better factor effects.

CHAPTER 5

Experimental work

The experiments were performed on ECOCUT CNC WEDM machine manufactured by Electronica at CTTC, Bhubaneswar. It is shown in Fig.5.1.

Fig.5.1 Wire EDM machine

The specification of wire EDM machine is give in the Table7. Fig. 5.2 shows the holding of the job on the work piece. Fig.5.3 shows the image of the work piece after each cut.

Table.5.1 Specification of wire EDM

Dielectric fluid	Distilled water
Maximum work piece size	400× 500 × 200µm
Maximum travel	250× 350 × 200mm
Manufacturers	Electronica

Fig.5.2 Aluminum work piece is cut by WEDM

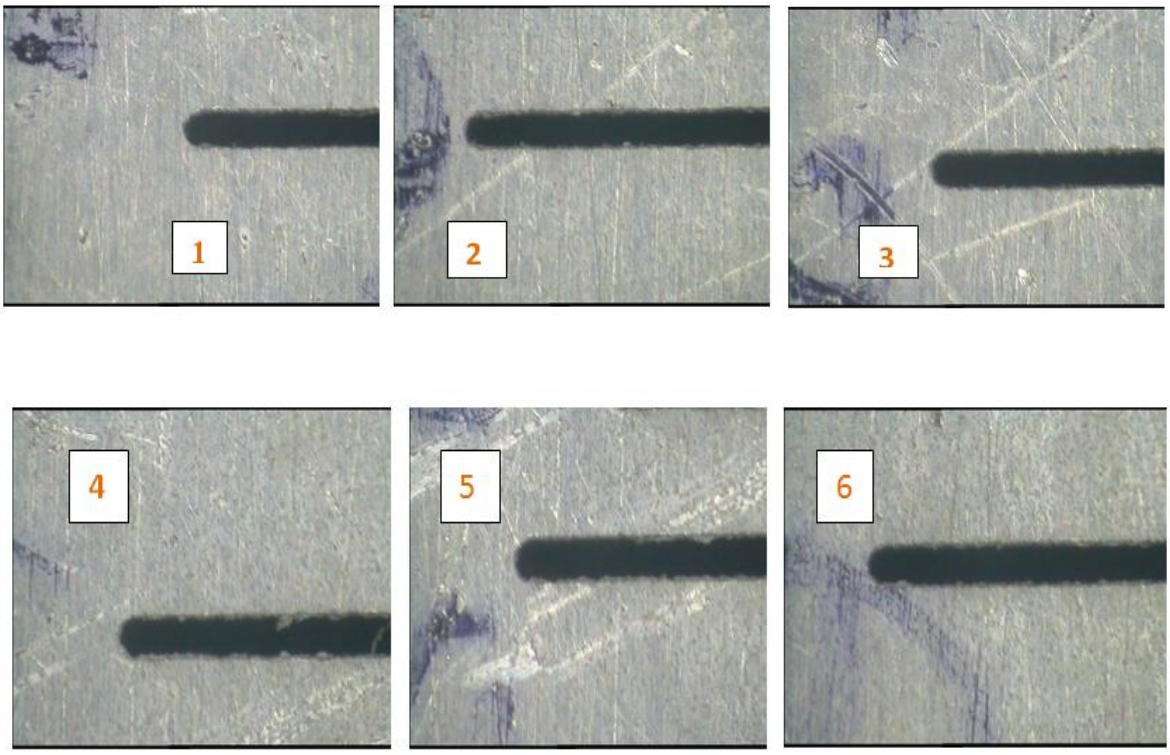

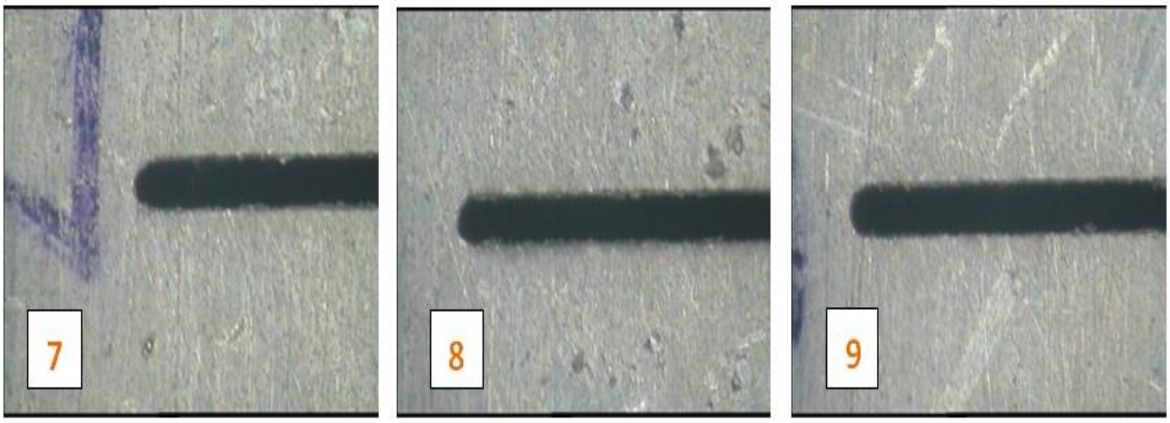

Fig5.3. Images of micro cut on the work piece

Table5.2. Constant machining parameter setting of WEDM

Parameter	Setting Value
Main Power Supply Voltage, V (Volt)	415V,3 phase
Servo Speed, SF (mm/min) at no load	Normal
Wire Tension, WT (g)	2
Wire Speed, WS (mm/min)	10
Flushing Pressure, FP (bar)	1
Wire diameter (mm)	0.25
Polarity	Work piece :+ve
Wire Electrode	Negative
Dielectric Fluid	Distilled water
Wire material	Brass Wire

5.1 Taguchi Design of experiments

Three control factors i.e. voltage, current and pulse on time were taken as input parameters. Each factor was put in three levels. The input parameters and their levels are given in table9. L9 orthogonal array was formed based on Taguchi optimization technique, which is shown in

Table10. The responses chosen for experiment were MRR, Kerf width and Cutting speed. The measured parameters from the experiment are given in the Table11.

Table.5.3 Process parameters and their levels

Process parameters	units	levels
Voltage	V	22, 24, 26
Current	A	1, 1.5, 2
Ton	µs	2, 5, 7

Table5.4.Orthogonal array (L_9) Taguchi design

No. of runs	Voltage (V)	Current (A)	Ton (µs)
1	22	1	2
2	22	1.5	5
3	22	2	7
4	24	1	5
5	24	1.5	7
6	24	2	2
7	26	1	7
8	26	1.5	2
9	26	2	5

Table5.5 Calculated experimental values of L_9 orthogonal array

No. of runs	Voltage (V)	Current (A)	Ton (µs)	MRR(mm^3/min)	Kerf Width (KW)	Cutting speed (S)
1	22	1	2	0.201	0.2888	10.7
2	22	1.5	5	0.169	0.27685	6.35
3	22	2	7	0.3089	0.2777	14.8
4	24	1	5	0.0175	0.2674	3.5
5	24	1.5	7	0.0477	0.2554	3.2
6	24	2	2	0.07	0.2503	10.55
7	26	1	7	0.07839	0.2794	11.55
8	26	1.5	2	0.2148	0.2725	8.95
9	26	2	5	0.1467	0.2691	6.65

CHAPTER 6

Results and discussions

6.1 ANSYS model confirmation

Before thermal modeling of Al work piece, the modeling of INCONEL718 was done to check the correctness of the present thermal modeling approach.

Table6.1 Process parameters used for modeling of INCONEL718 material

Process parameters	Values	units
Voltage	30	V
Current	2	A
Heat input to the work piece	0.2	
Spark radius	5	µm
Pulse-on time	2	µs
Pulse-off time	100	µs

The comparison results of the two developed models for INCONEL718 with V=25V, I=4A and P=0.20are shown in Fig.6.1 and Fig.6.2.

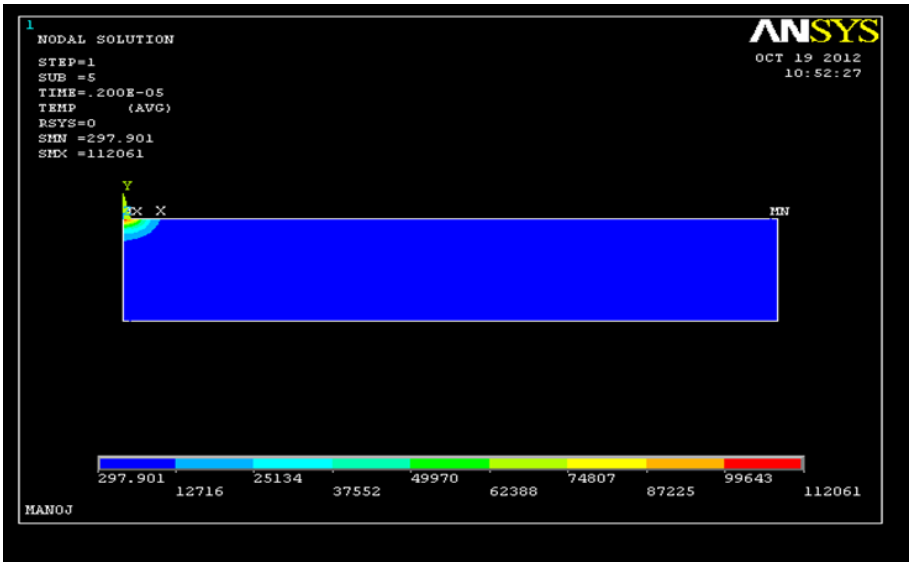

Fig.6.1 Temperature distribution of earlier developed model for INCONEL 718 [28]

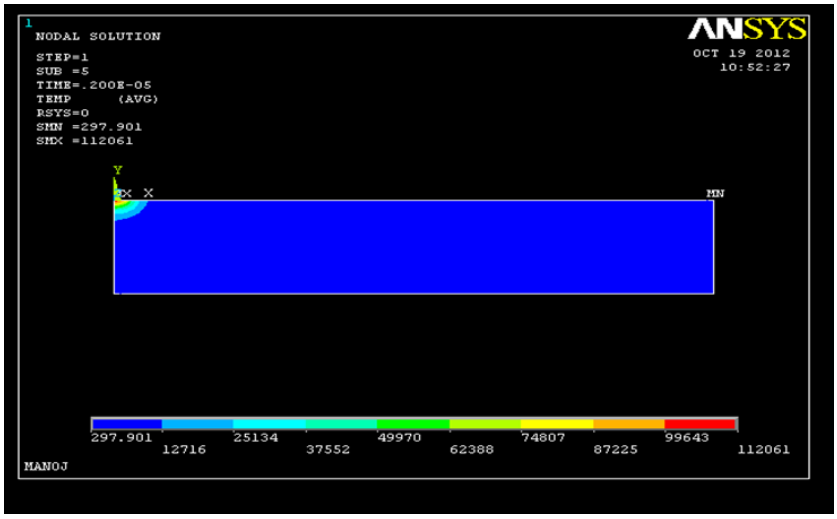

Fig.6.2 our developed thermal modeling for inconel718 material

From Fig.6.1 and Fig.6.2, it is seen that the maximum temperature reached by our model is approaches to the previously developed model [3]. Hence it is concluded that the modeling process followed by us is correct.

Table.6.2 properties of Aluminum (Al) work piece

Material properties	value	unit
Thermal conductivity (K)	205	W/m-K
Specific heat (C)	910	kJ/kg-K
Density (ρ)	2700	Kg/m^3
Melting point (t)	923	K
Young's modulus (E)	70	GPa
Poisson's ratio (μ)	0.33	

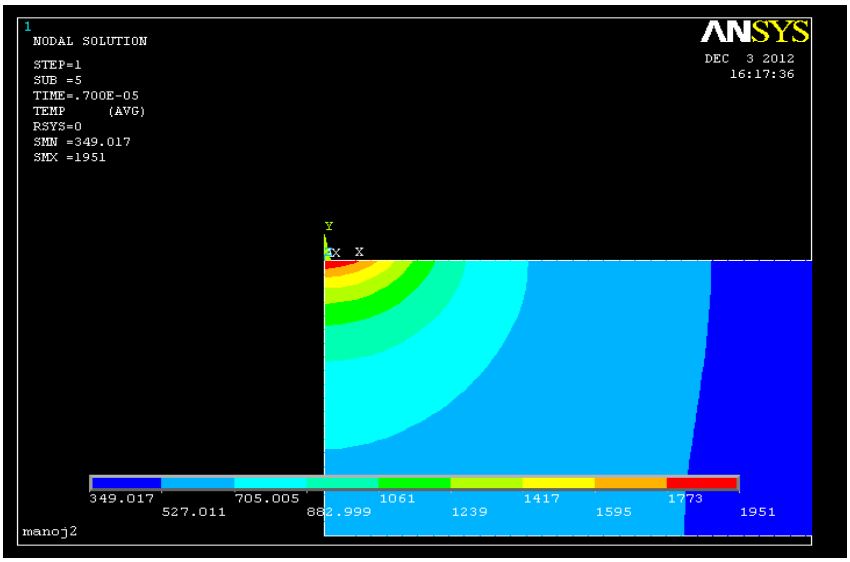

Fig. 6.3 Temperature distribution in Aluminum (Al) work piece with V=22V, I=1.5A and P=0.2

Fig.6.3 is the temperature distribution of Al work piece. Maximum temperature reached is located at the Centre, where the intensity of heat flux is maximum. The magnitude of

temperature decreases as the distance increases from the Centre line. Study from the Fig. 6.3 reveals that the distribution of temperature is divided in to four distinct regions. They are

i. Boiling region (red region)
ii. Liquid region (up to light green colour)
iii. HAZ (up to light blue colour)
iv. Solid metal (blue colour)

Thermal modeling, modeling of residual stress had been done, and modeling of MRR and its values were estimated theoretically for Aluminum (Al) work piece. Three process parameters i.e. voltage, current and pulse on time (Ton) with each having three levels were set at L9 orthogonal array. For this Taguchi experimental design method was adopted and for that MINITAB16 software was used. Theoretical values were estimated for each run order. Properties of Al work piece are shown in table 3. Process parameters and their levels are shown in Fig.4 and L9 orthogonal array is shown in table 5.

Table6.3 L9 orthogonal array

No. of runs	Voltage (V)	Current (A)	Ton (µs)
1	22	1	2
2	22	1.5	5
3	22	2	7
4	24	1	5
5	24	1.5	7
6	24	2	2
7	26	1	7
8	26	1.5	2
9	26	2	5

6.2 Thermal modeling of micro wire EDM for single spark

After the result was verified by INCONEL718 material, thermal modeling has been done for Al work piece with respect to the process parameters shown in Table 5. The study of *Pandey and Jilani* [20] for die-sinking EDM reveals that the value of energy distribution factor (Fc) should be 0.08 to 0.2. Within this range of Fc the theoretical modeled values are closer to the experimental value. For our modeling the value of Fc was varied within the range of 0.08-0.2. The results of the predicted thermal model have shown from Fig6.4 to Fig6.10.

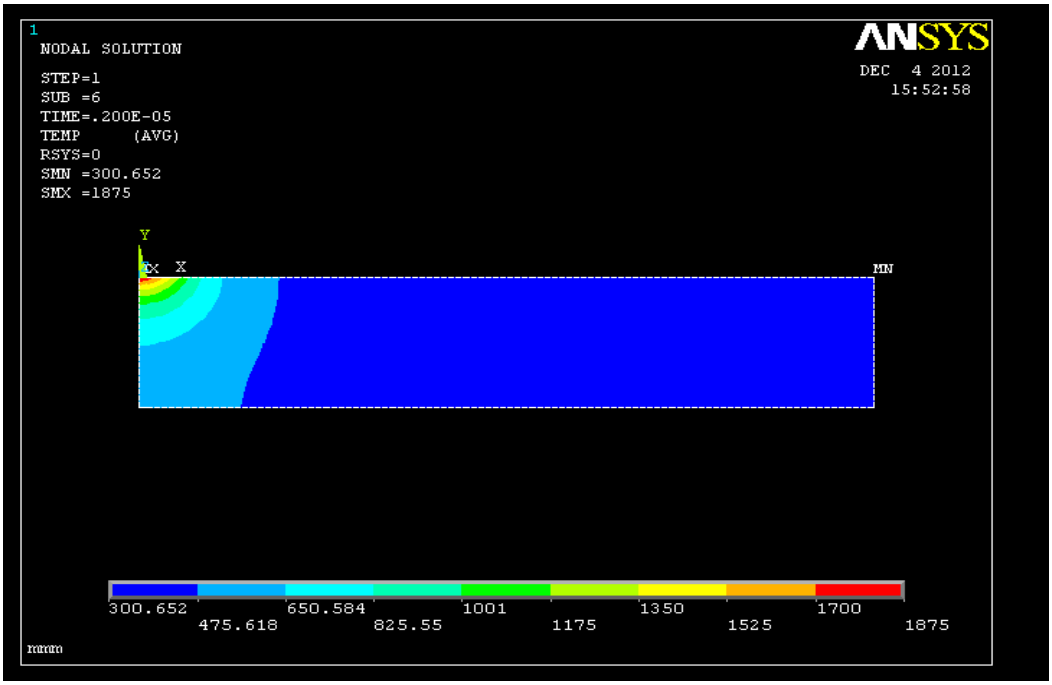

Fig.6.4 Temperature distribution in Aluminum (Al) work piece with V=22V, I=1A and P=0.08

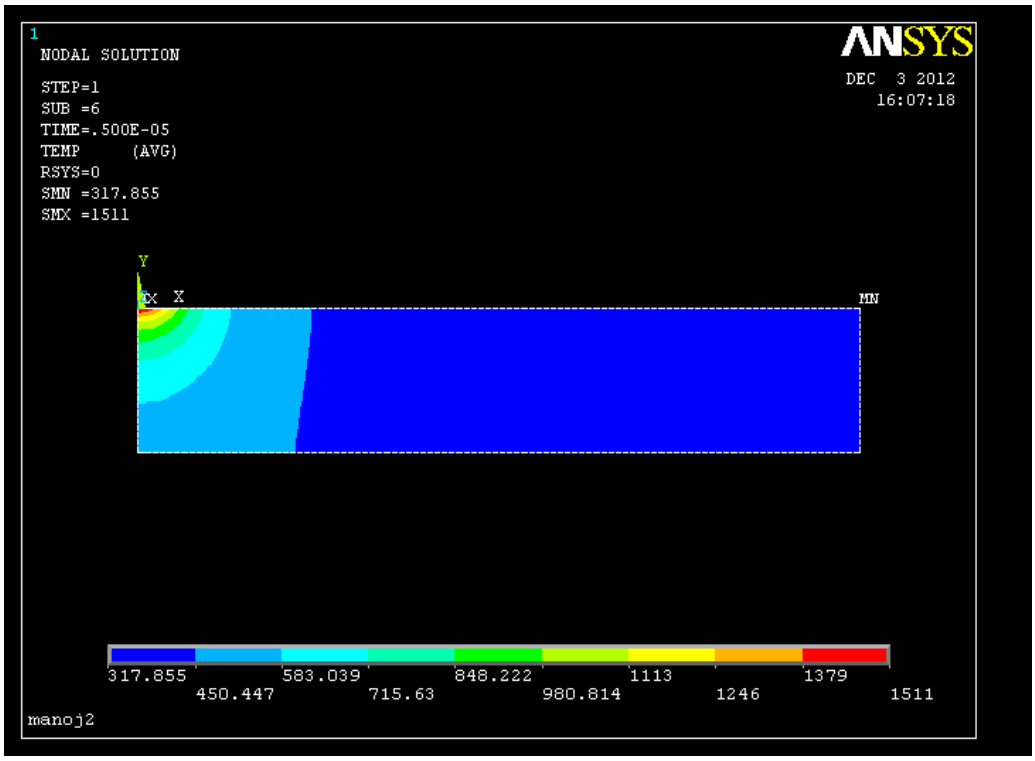

Fig.6.5 Temperature distribution in Aluminum (Al) work piece with V=22V, I=1.5A and P=0.15

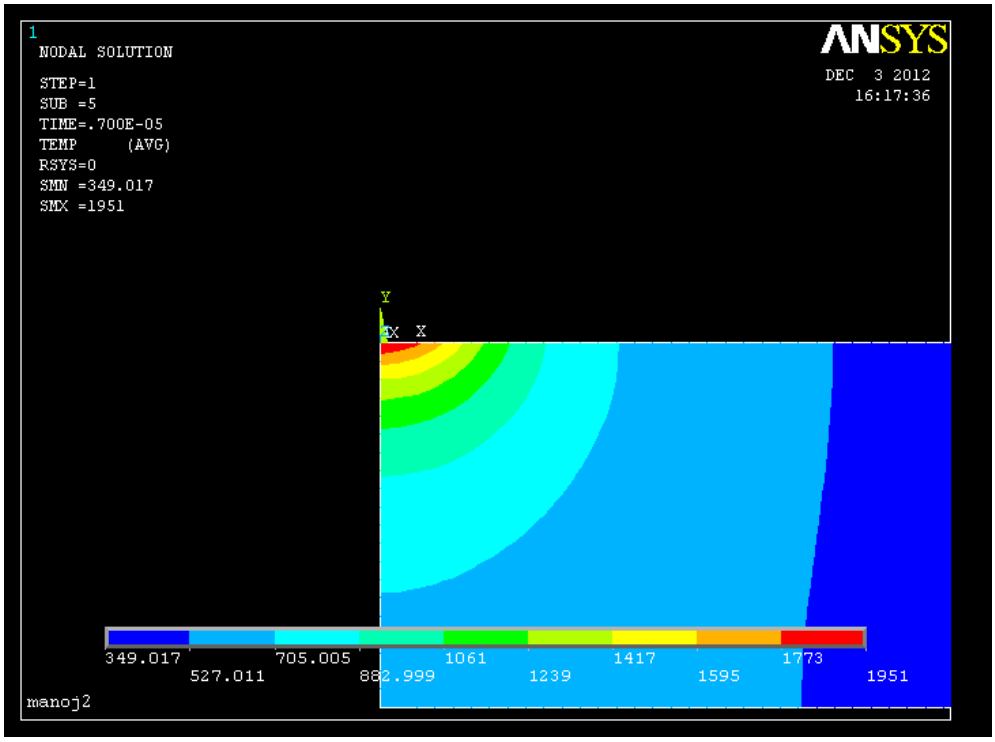

Fig.6.6 Temperature distribution in Aluminum (Al) work piece with V=22V, I=2A and P=0.2

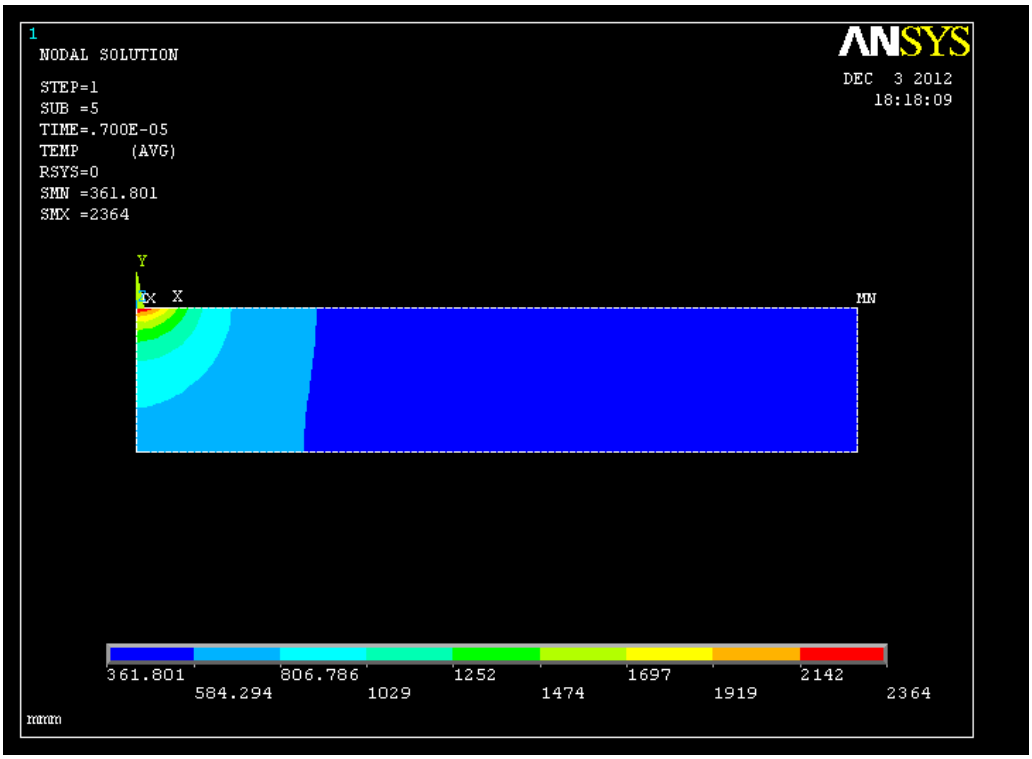

Fig.6.7 Temperature distribution in Aluminum (Al) work piece with V=24V, I=1.5A and P=0.08

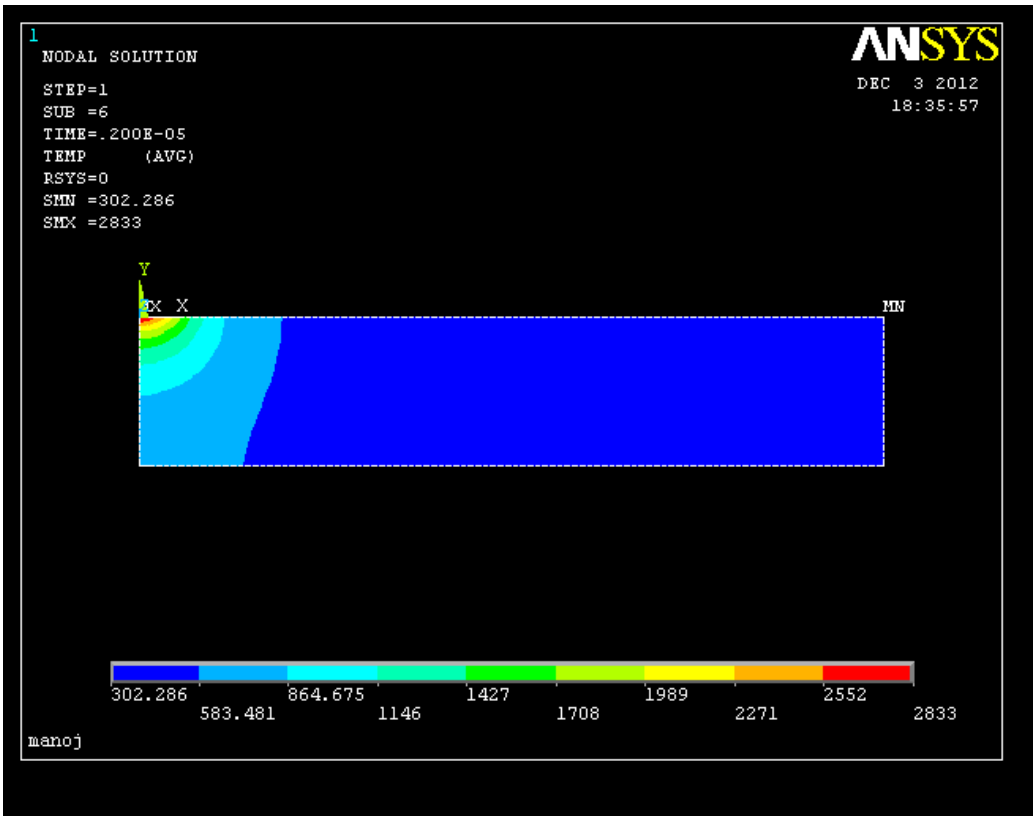

Fig.6.8 Temperature distribution in Aluminum (Al) work piece with V=24V, I=2A and P=0.15

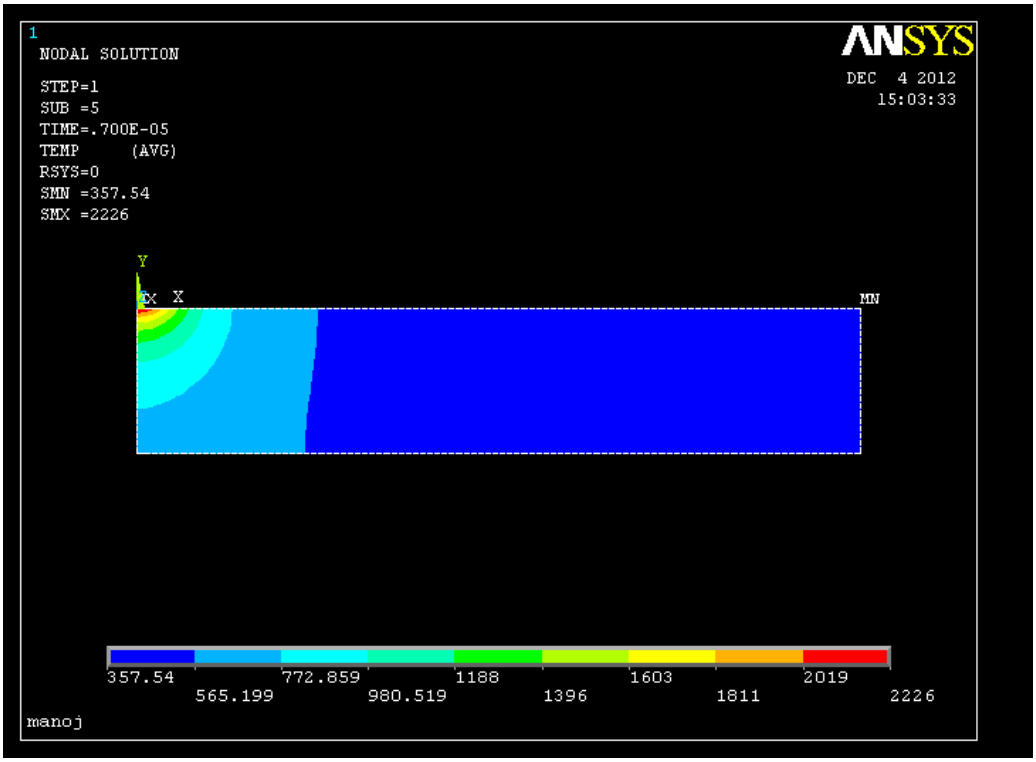

Fig.6.9 Temperature distribution in Aluminum (Al) work piece with V=26V, I=1A and P=0.15

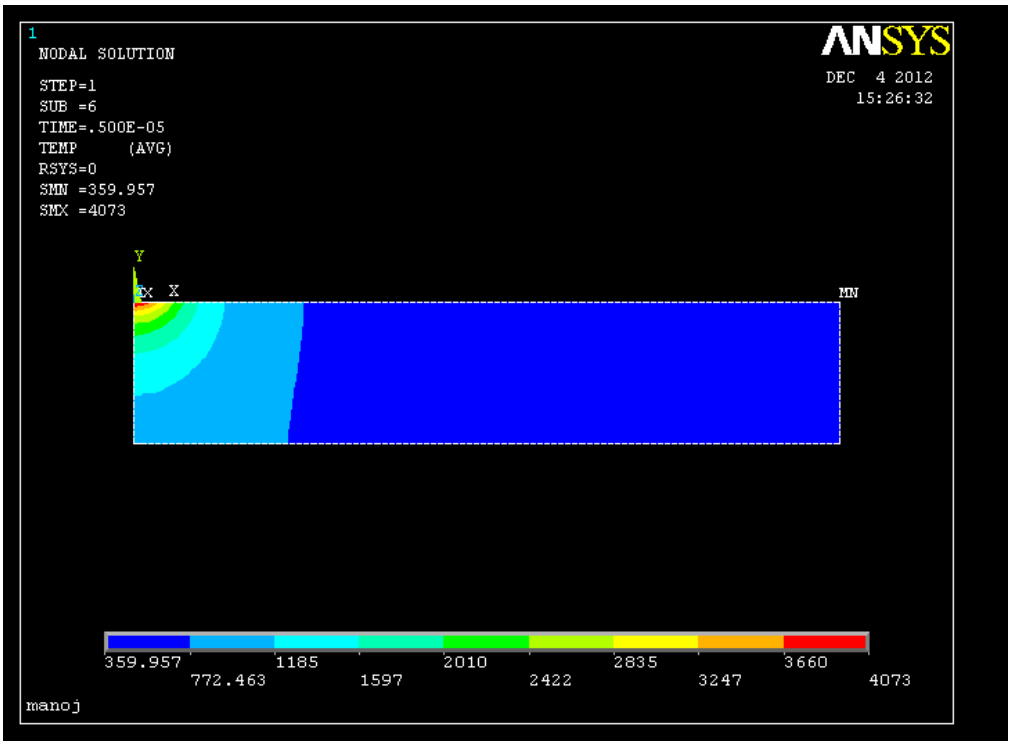

Fig.6.10 Temperature distribution in Aluminum (Al) work piece with V=26V, I=2A and P=0.08

6.3 Modeling results of MRR for micro wire EDM

After thermal modeling was done the materials above the melting point temperature were removed by killing the elements. Death/ birth option was used for that. The value of MRR will be estimated using Eq.5 and Eq.6 The modeling results of MRR are shown in Fig6.11 to Fig6.19.

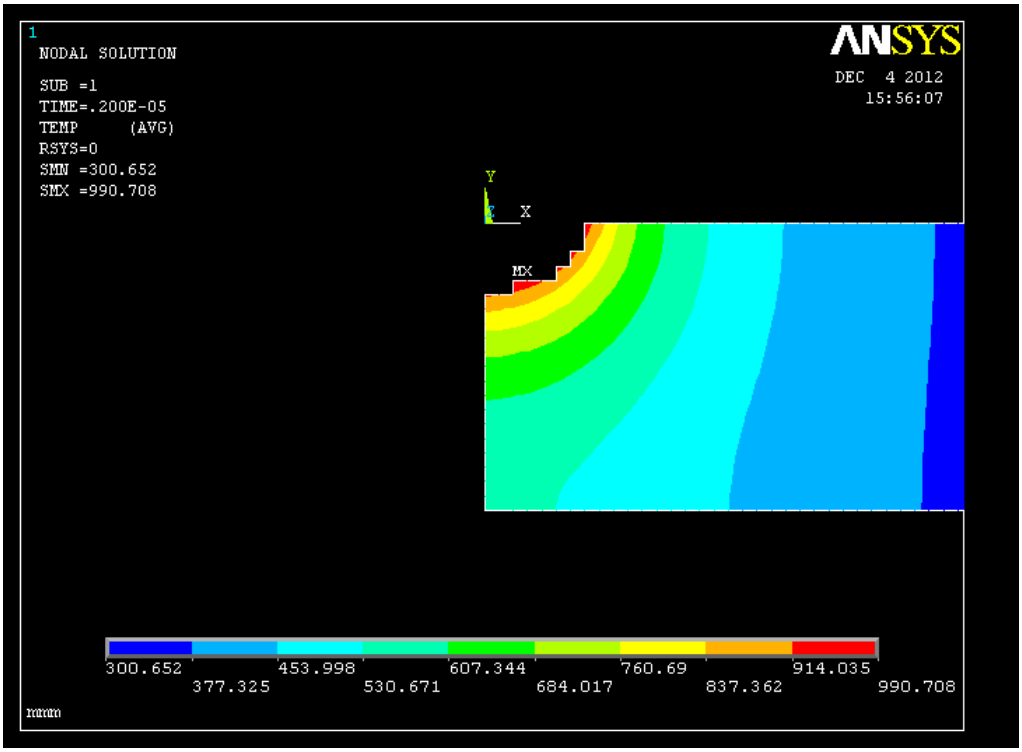

Fig.6.11 Temperature distribution in Al work piece with after material was removed V=22V, I=1A and P=0.08

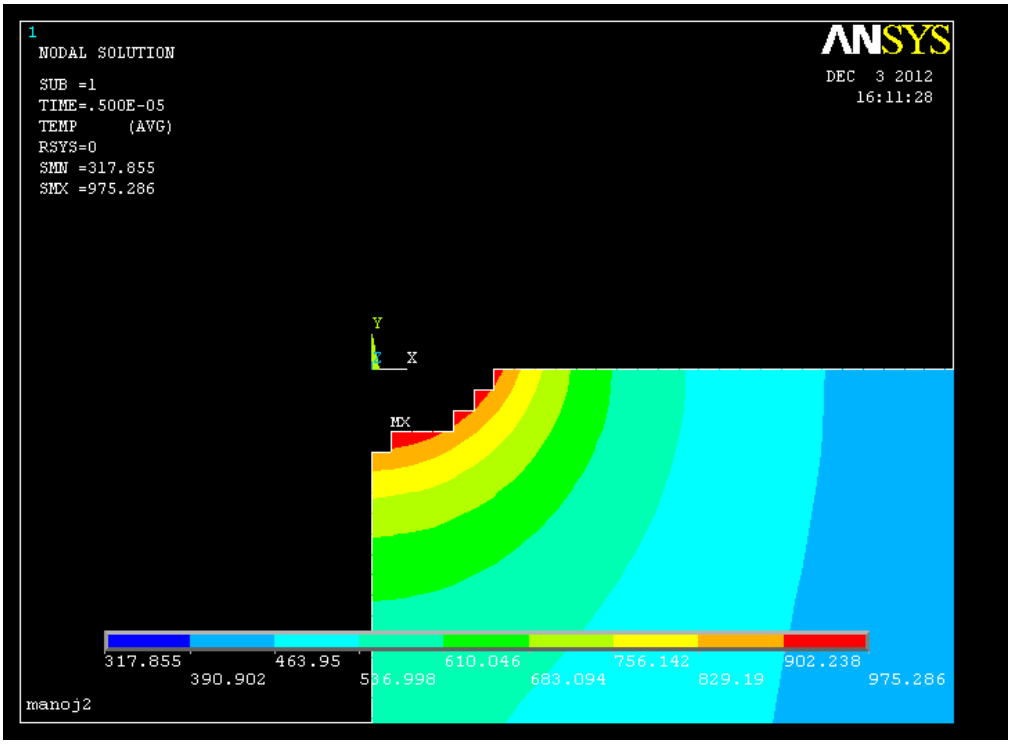

Fig.6.12 Temperature distribution in Al work piece with after material was removed V=22V, I=1.5A and P=0.15

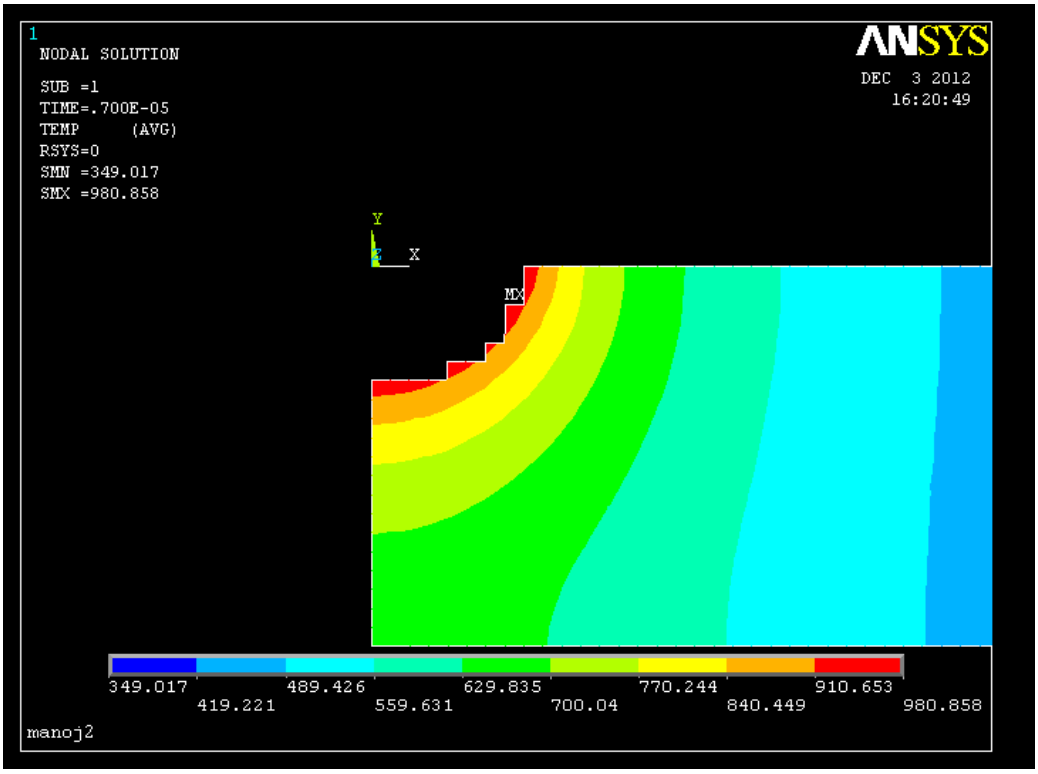

Fig.6.13 Temperature distribution in Al work piece with after material was removed V=22V, I=2A and P=0.15

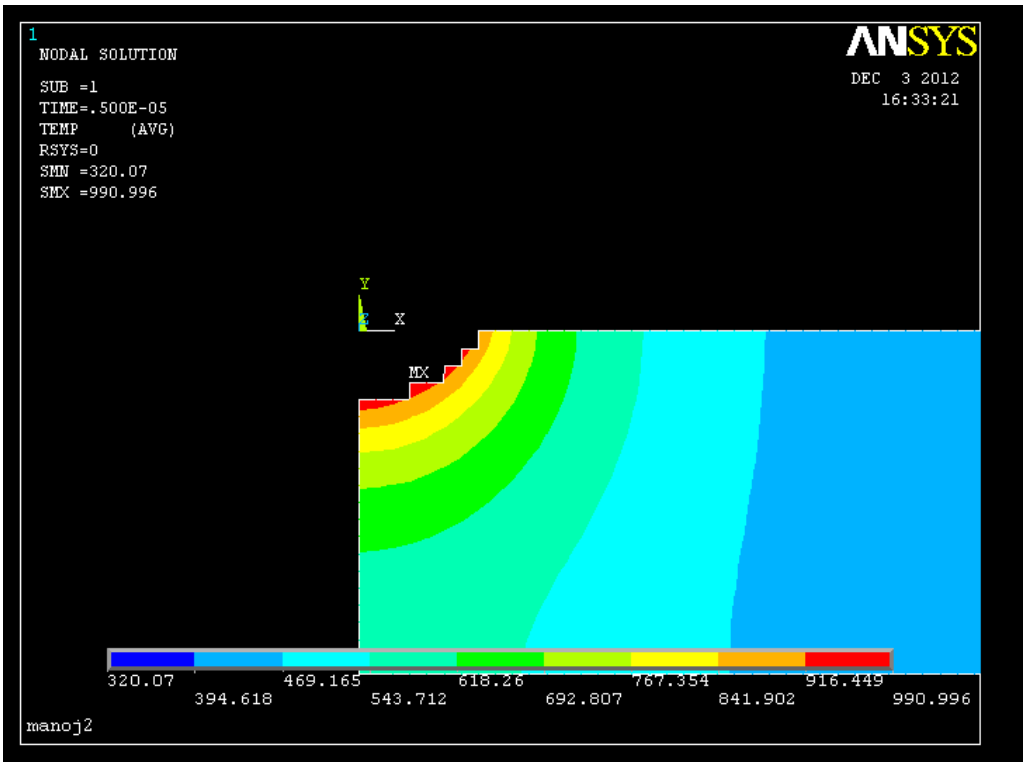

Fig.6.14 Temperature distribution in Al work piece with after material was removed V=24V, I=1A and P=0.2

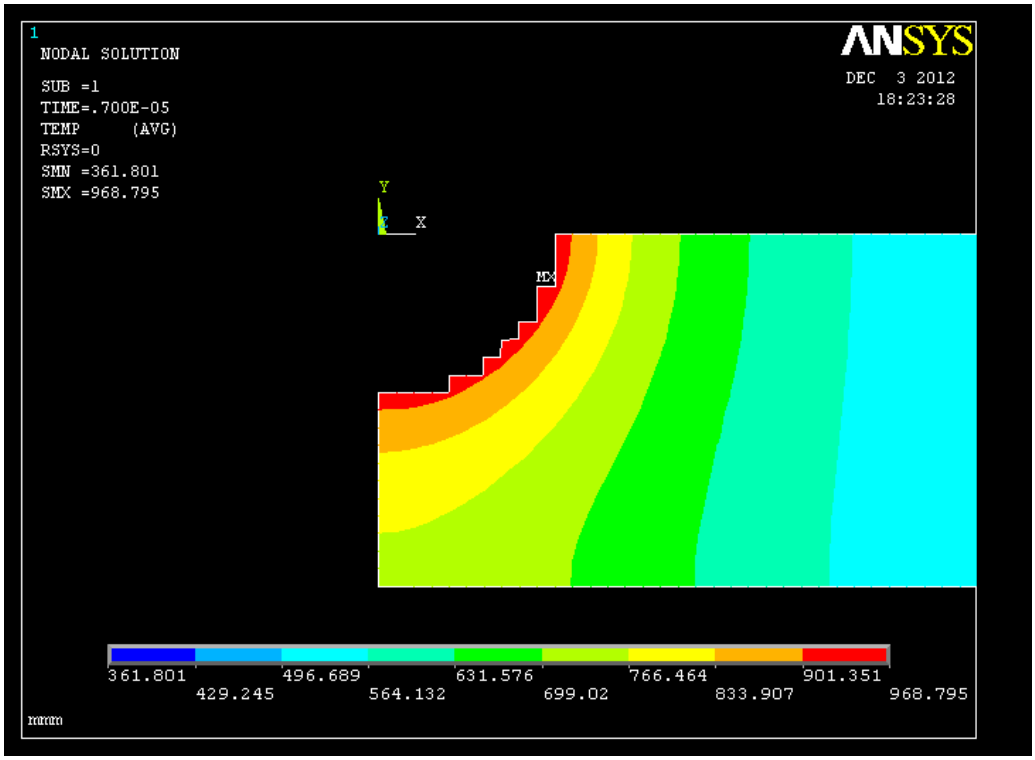

Fig.6.15 Temperature distribution in Al work piece with after material was removed V=24V, I=1.5A and P=0.08

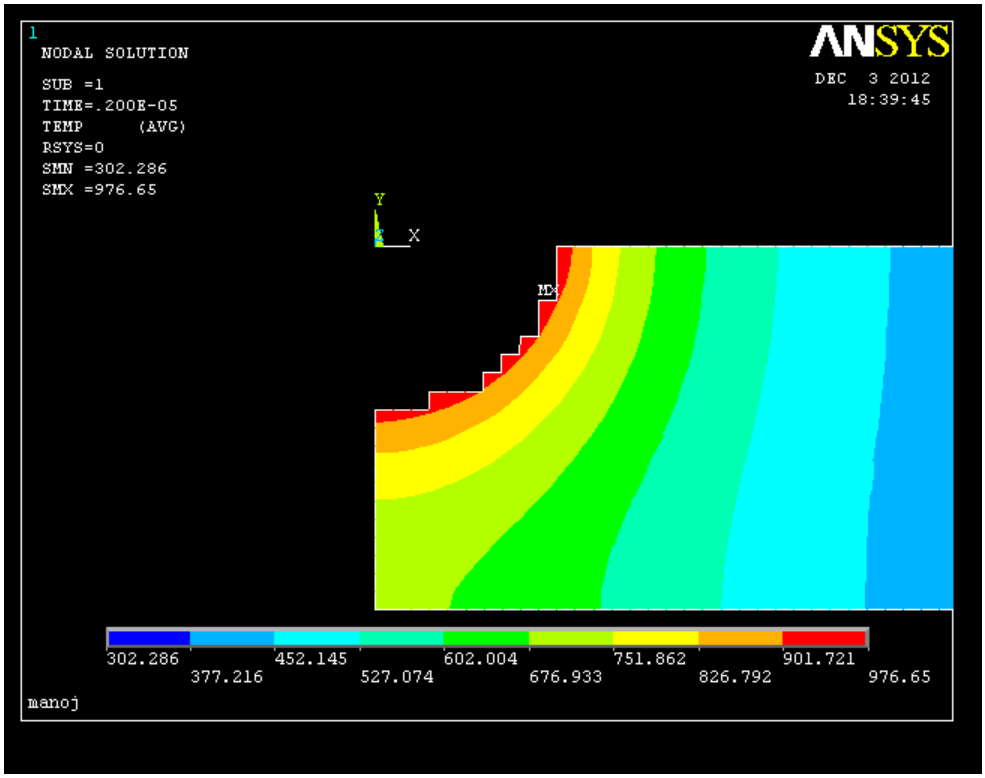

Fig.6.16 Temperature distribution in Al work piece with after material was removed V=24V, I=2A and P=0.15

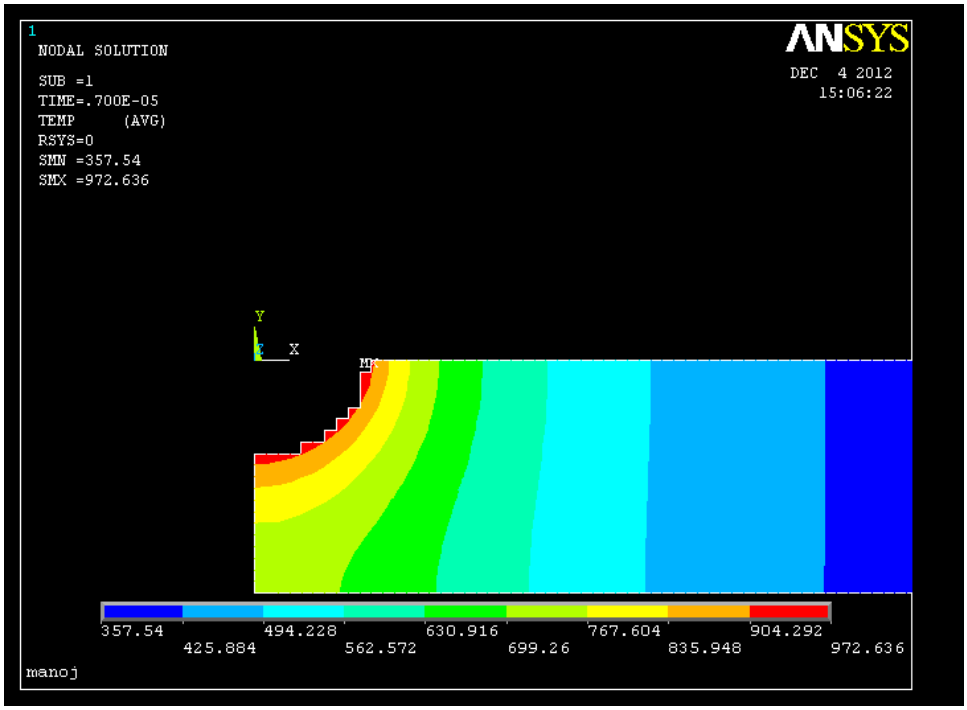

Fig.6.17Temperature distribution in Al work piece with after material was removed V=26V, I=1A and P=0.15

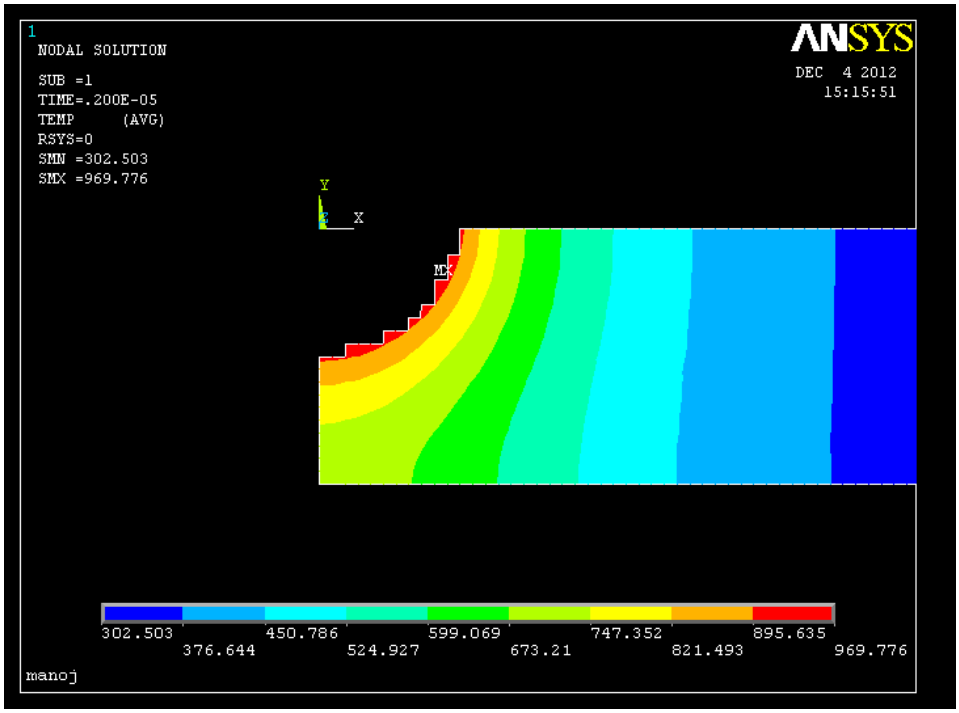

Fig.6.18 Temperature distribution in Al work piece with after material was removed V=26V, I=1.5A and P=0.2

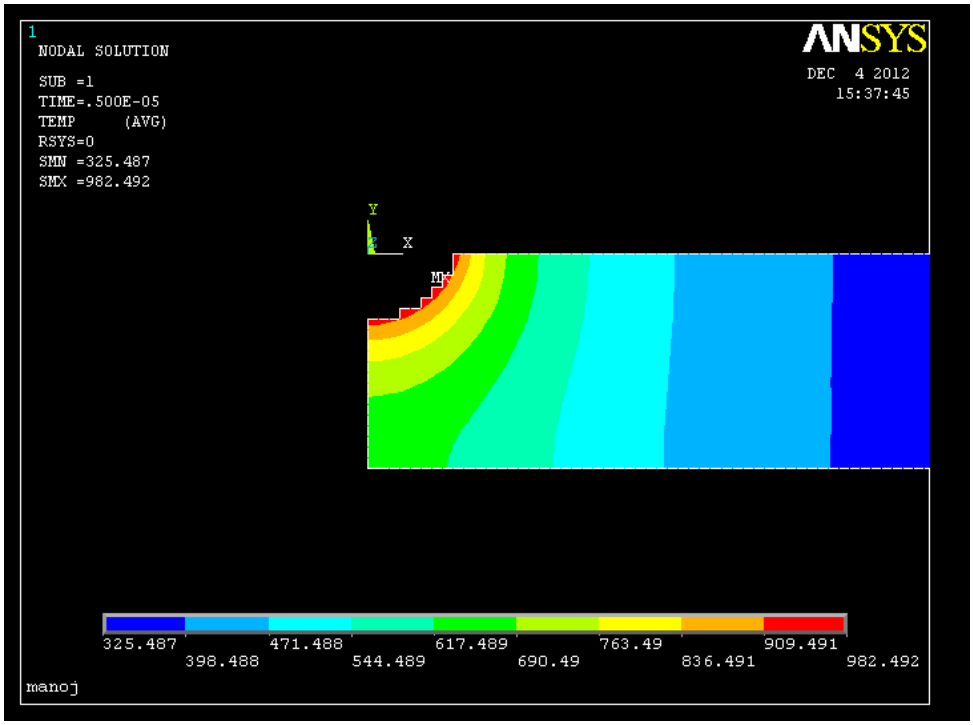

Fig.6.19 Temperature distribution in Al work piece with after material was removed V=26V, I=2A and P=0.8

6.4 Modeling results of Residual Stress modeling for micro wire EDM

Residual stress is developed due to thermal shrinkage during solidification. Due to residual stress deformation takes place on the surface of the work piece, which affects the machining accuracy. Purpose of Micro wire EDM is to machine the work piece with high accuracy and tolerance, hence the residual stress developed on the machined component should be minimized. Modeled results of residual stress with same process parameters as that of thermal modeling for 100µm are shown in Fig.6.20 to Fig.6.27.

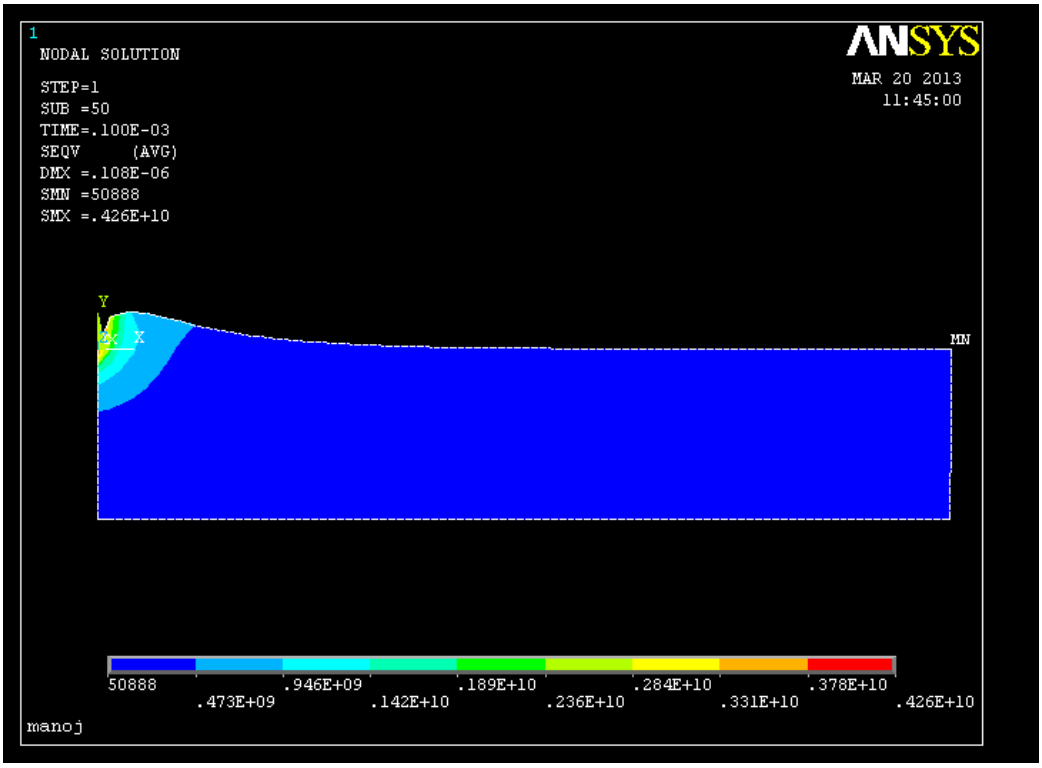

Fig.6.20 Distribution of residual stress of Al at V=22V, I=1A and P=0.08

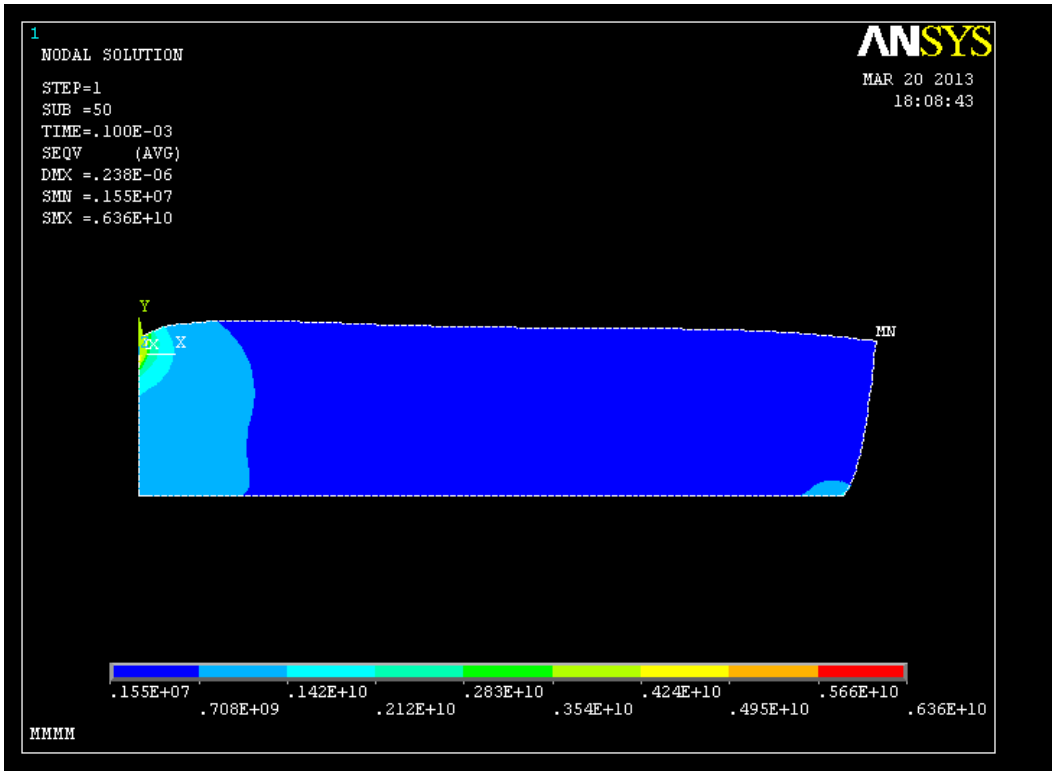

Fig.6.21 Distribution of residual stress of Al at V=22V, I=1.5A and P=0.15

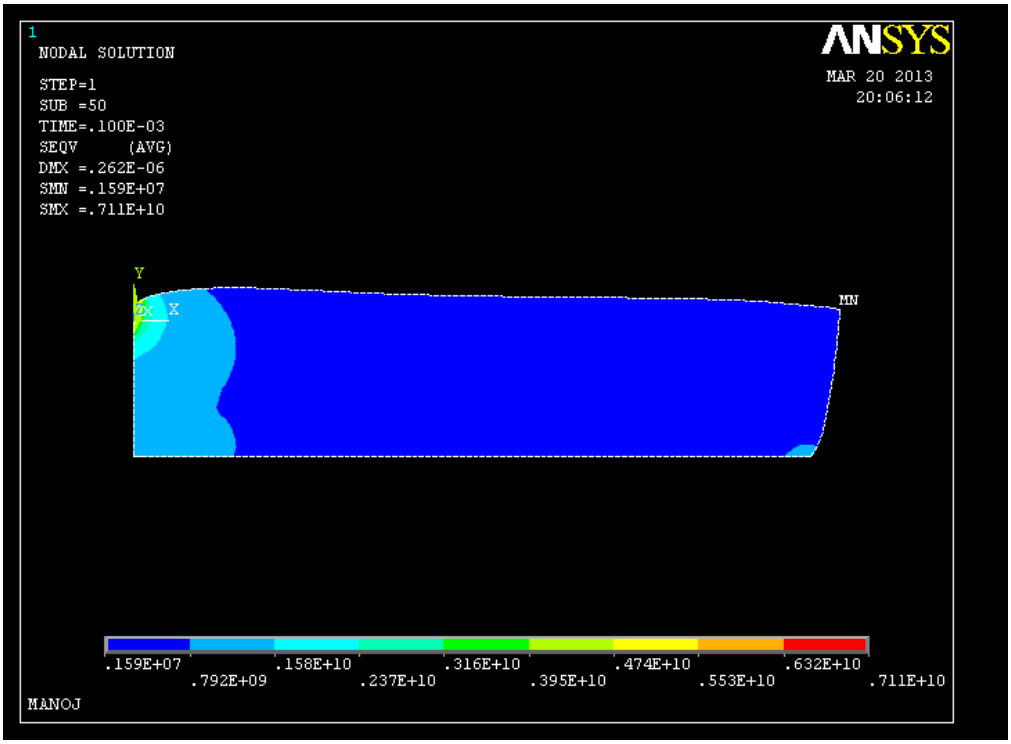

Fig.6.22 Distribution of residual stress of Al at V=22V, I=2A and P=0.2

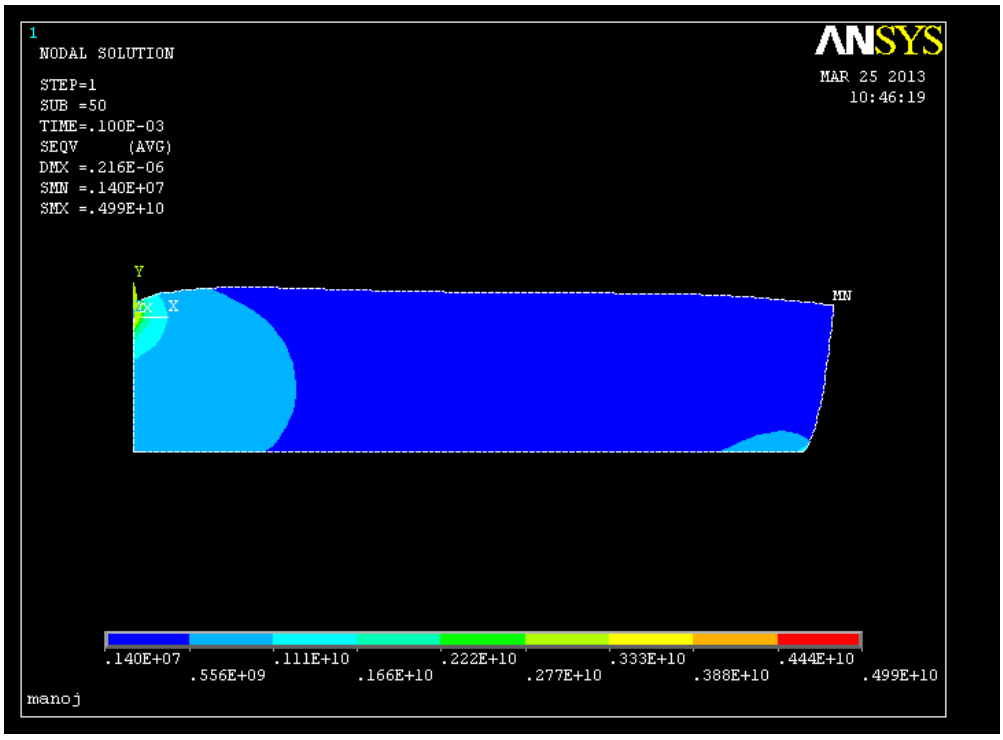

Fig.6.23 Distribution of residual stress of Al at V=24V, I=1A and P=0.2

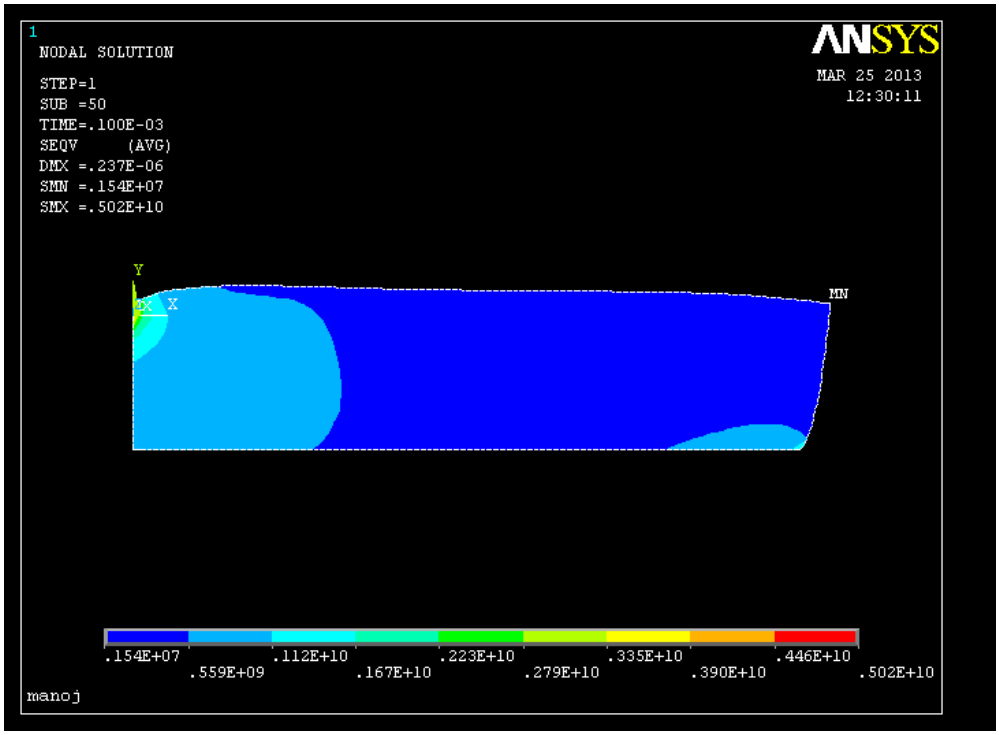

Fig.6.24 Distribution of residual stress of Al at V=24V, I=2A and P=0.15

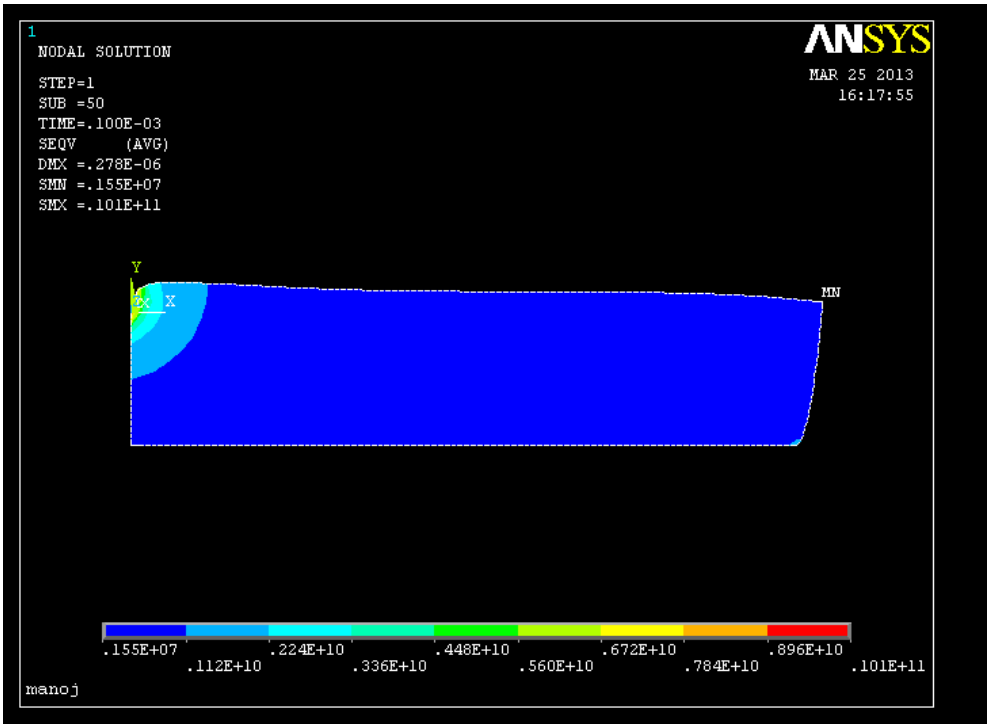

Fig.6.25 Distribution of residual stress of Al at V=24V, I=1.5A and P=0.08

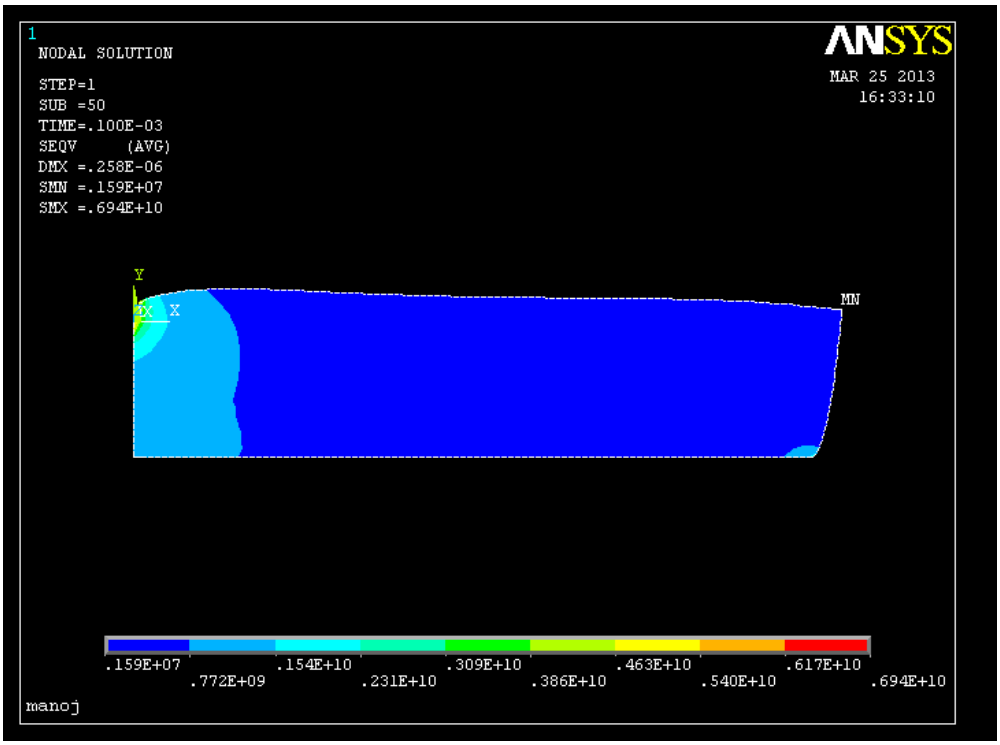

Fig.6.26 Distribution of residual stress of Al V=26V, I=1A and P=0.15

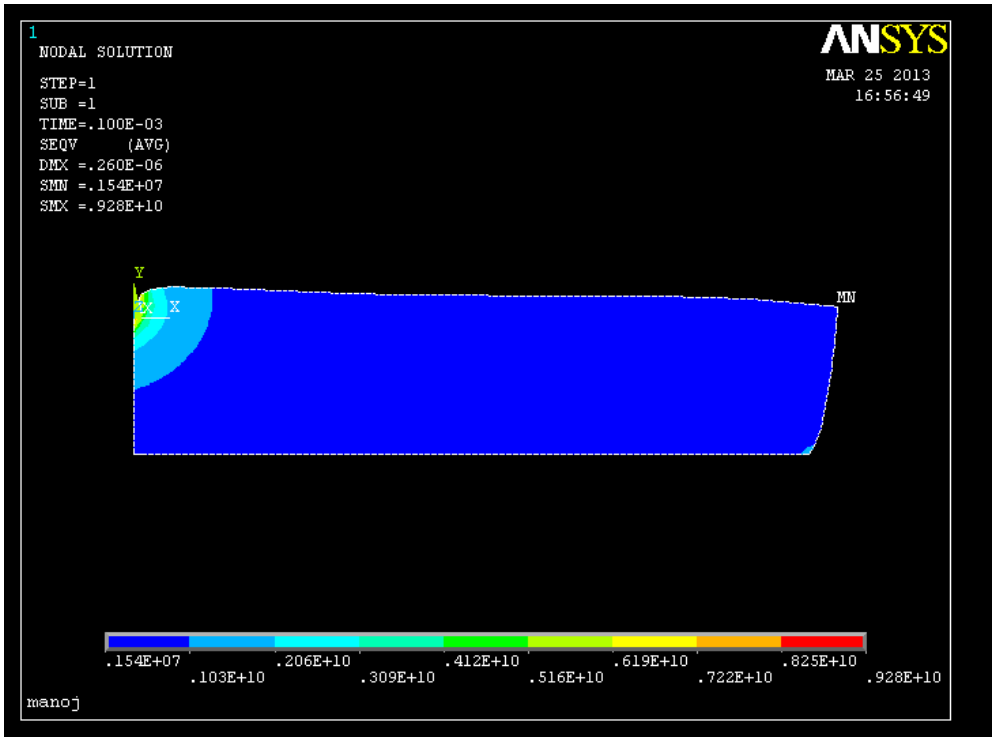

Fig.6.27 Distribution of residual stress of Al V=26V, I=1.5A and P=0.2

6.5 Modeling Results

The values of modeling results for MRR and residual stress are given in the table.6 MRR values were obtained by using Eq.11 to Eq.14.and residual stress values were obtained from the model.

Table6.4 Theoretical results obtained from ANSYS modeling

Si. No.	MRR(mm^3/min)	Residual Stress(GPa)
1	0.251	4.26
2	0.1372	6.36
3	0.3653	7.11
4	0.01628	4.99
5	0.0562	5.02
6	0.0562	10.1
7	0.09661	6.94
8	0.2410	9.28
9	0.1314	8.2

6.6 Comparison between theoretical and experimental results.

In this section the comparison has been done between theoretical and experimental material removal rate (MRR). Theoretical MRR has been estimated by FEA modeling.

Table6.5 Comparison of theoretical and experimental MRR

Si no	Voltage (V)	Current (I)	Ton	Fc	Theo. MRR (mm^3/min)	Exp. MRR (mm^3/min)	% error
1	22	1.0	2	0.20	0.251	0.201	24.80
2	22	1.5	5	0.13	0.137	0.169	-18.82
3	22	2.0	7	0.11	0.365	0.308	18.25
4	24	1.0	5	0.13	0.016	0.017	6.97
5	24	1.5	7	0.08	0.056	0.047	17.82
6	24	2.0	2	0.18	0.056	0.070	-19.71
7	26	1.0	7	0.18	0.096	0.078	23.24
8	26	1.5	2	0.20	0.241	0.214	12.19
9	26	2.0	5	0.08	0.131	0.146	-10.42

6.7 Effect of different process parameters

6.7.1 Effect of Voltage

From the Fig.42 and Fig.43, it is observe that top surface temperatures go on increasing with increase in current. It happens due to voltage is a function of heat energy transferred to the work piece, i.e. larger the current greater the heat energy generated and transferred to the work

piece. Again it can be seen from Fig.6.28 that temperature follows the shape of Gaussian curve. The temperature decreases further as the distance from the work piece increases.

From Fig.6.29, it is observed that temperature is maximum at the top surface and decreases as we proceed down words. Work piece temperature till 4µm reduces very sharply. Mostly residual stress developed in this region only because in this region difference of temperature is higher. It is concluded from this analysis is that more materials are removed along the radius compared to the depth. Hence it is predicted that a shallow crater is formed during machining.

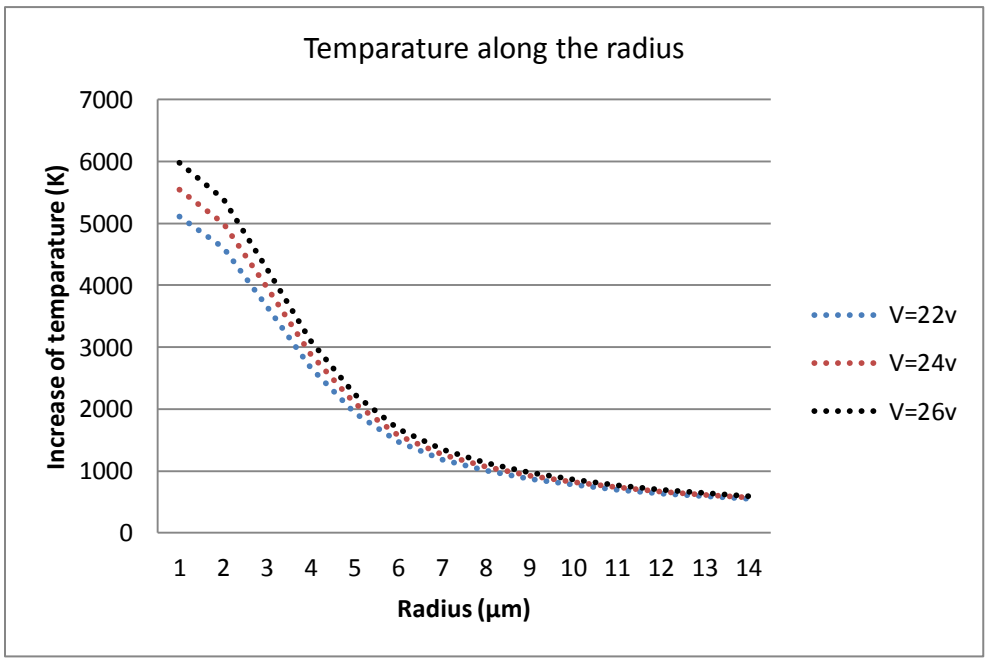

Fig6.28 The effect of current (I) on the temperature distribution along the radius of the work piece for Al at I=2A, Ton=2µs, P=0.2

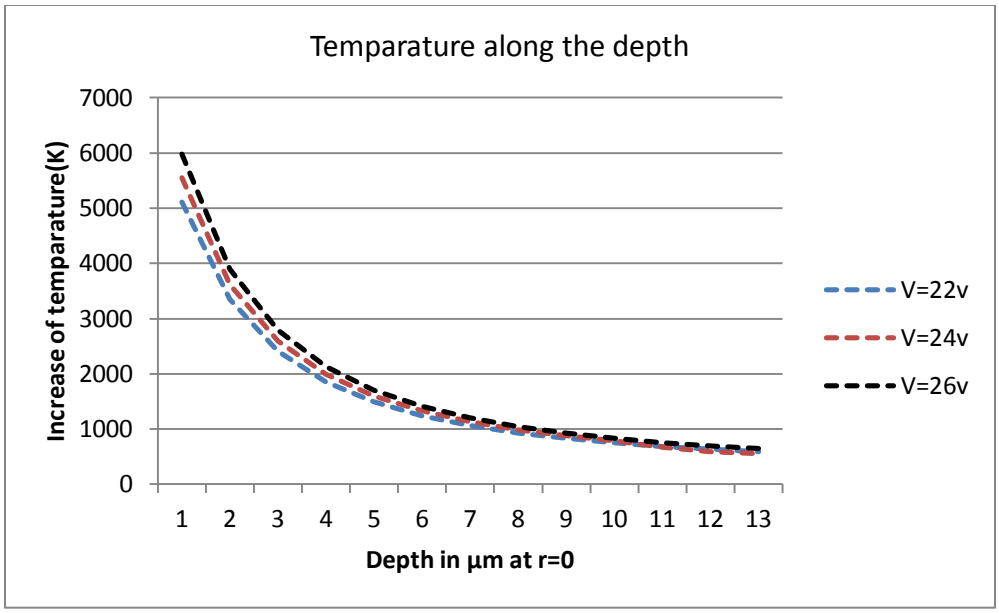

Fig.6.29 The effect of current (I) on the temperature distribution along the depth of the work piece for Al at I=2A, Ton=2µs, P=0.2

6.7.2 Effect of Current

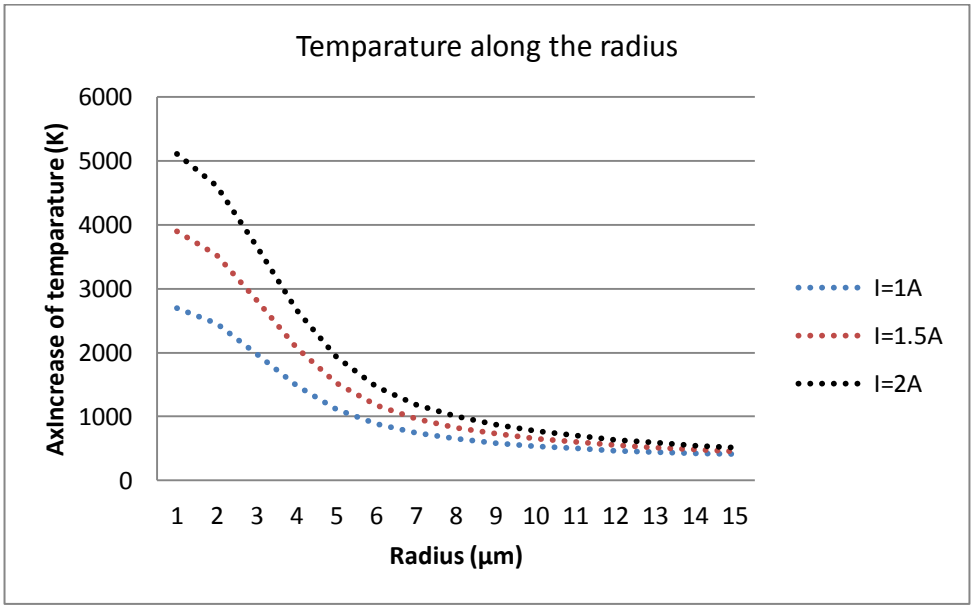

Fig.6.30 The effect of current (I) on the temperature distribution along the radius of the work piece for Al at V=22v, Ton=2µs, P=0.2

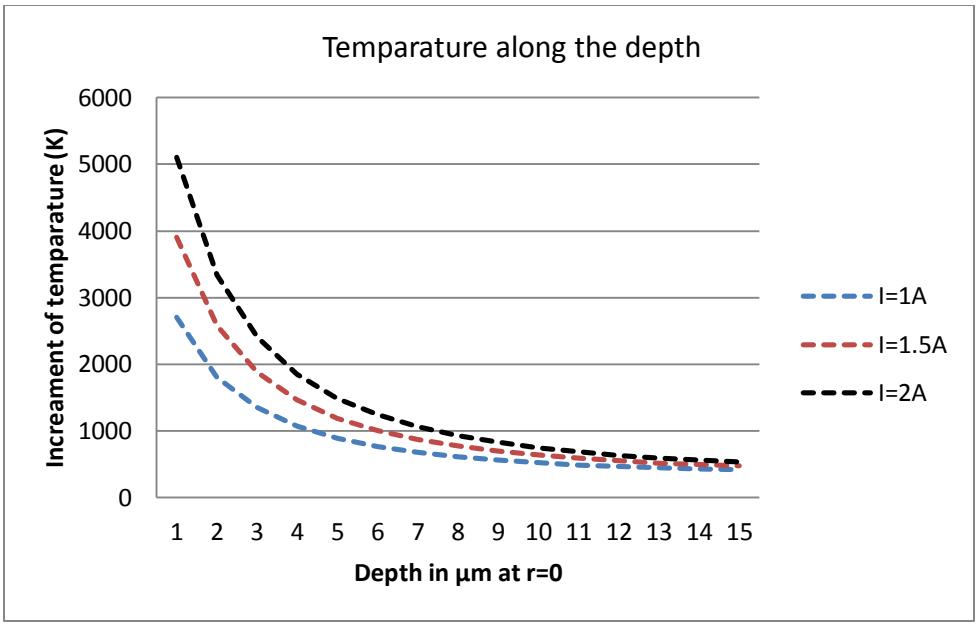

Fig.6.31 The effect of current (I) on the temperature distribution along the depth of the work piece for Al at V=22v, Ton=2µs, P=0.2

The variation of temperature along the radius and depth the work piece is shown in Fig.6.20 and Fig.6.21 respectively. From the trend of variation of surface temperature, it is observed that the surface temperature increases with the increase of current. It is seen from the Fig.6.20 that the curve is steep up to 8µm. it is also seen that with a small variation of current the variation of maximum temperature is higher.

From Fig.6.21 it is seen that as the current increases the temperature inside the work piece increases irrespective of length. Temperature gradient is higher up to 5µm and further increases of depth the variation of temperature is almost constant. Since the distance of temperature gradient is more along the radius a shallow bowl shaped crater is formed during machining.

6.7.3 Effect of pulse duration (Ton)

Effects of variation in pulse duration on the surface temperature distribution in micro wire EDM along the radius and depth are plotted in Fig.6.22 and Fig.6.23. From the trend of variation of surface temperature along the radius of the work piece (Fig.6.22), it is seen that surface the temperature increases with the increase of pulse duration (Ton). This happens because if the heat is supplied for longer period of time, the temperature will also be higher. Further it is observed that at the spark location, temperature reached is maximum and it moves down as the distances along the surface is increased. The variation of temperature is less up to the distance 2µm and is increases up to 7µm; rate of decrement of temperature is almost constant beyond 7µm.

Fig.6.23 reveals that temperature gradient is steeper than the variation of temperature along the radius. The reduction of temperature is higher at lower value of pulse on time. It may be drawn from the graph that, at the lower pulse duration heat dissipation to the surrounding is less than the large pulse duration.

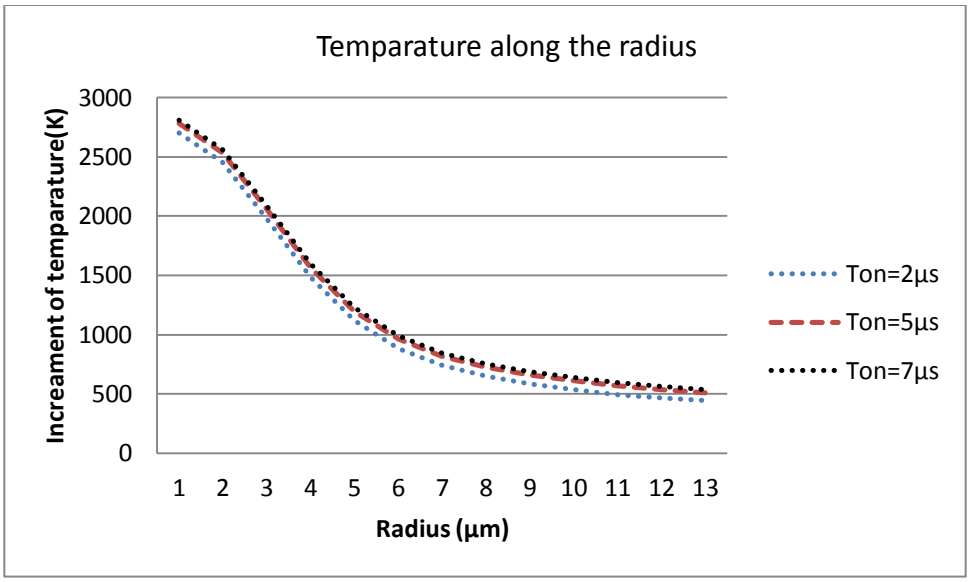

Fig.6.32 The effect of Ton on the temperature distribution along the radius of the Al work piece at V=22v,I=1.0A, P=0.2

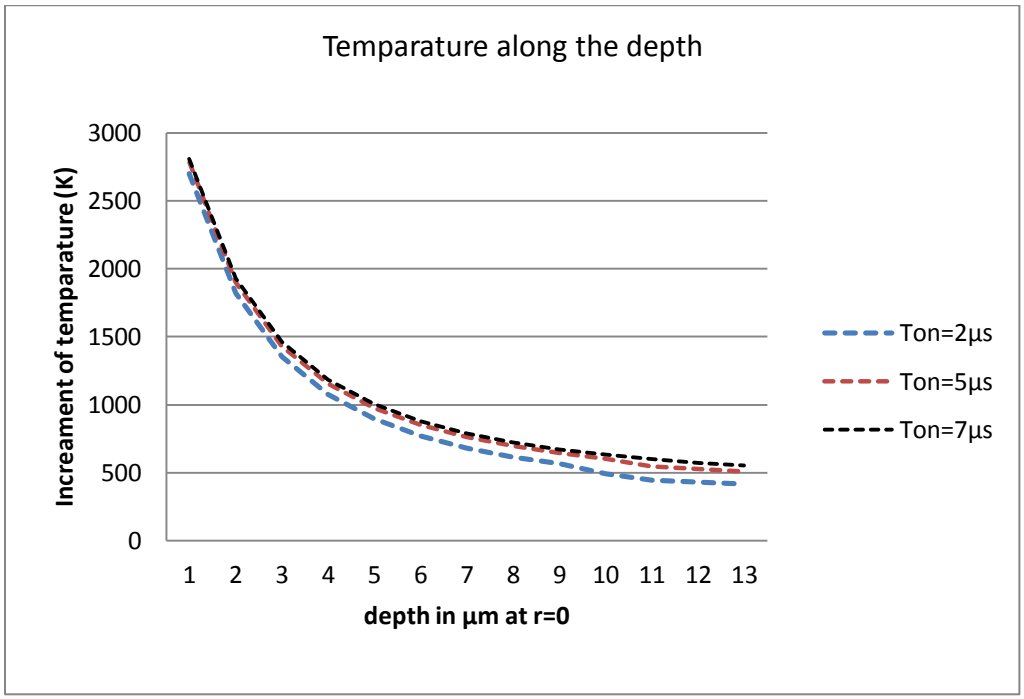

Fig.6.33 The effect of Ton time on the temperature distribution along the depth of the work piece for Al at V=22v, I=1.0A, P=0.2

6.8 Weighted Principal Component Analysis (WPCA) Results

Table 12 shows the S/N ratios of each response and their corresponding normalized S/N ratio values.

Table6.6 S/N ratio and normalize S/N ratio values of (MRR, KW, S)

Si. No	SNRA1	SNRA2	SNRA3	NOR SNRA1	NOR SNRA2	NOR SNRA3
1	-13.9361	10.7881	20.5877	0.85031441	0	0.78819293
2	-15.4423	11.1551	16.0555	0.78991081	0.295324696	0.447482371
3	-10.2036	11.1285	23.4052	1	0.273919691	1
4	-35.1392	11.4568	10.8814	0	0.538102519	0.058516636
5	-26.4296	11.8556	10.103	0.34928375	0.859016657	0
6	-23.098	12.0308	20.465	0.48289193	1	0.778968892
7	-22.1148	11.0755	21.2516	0.5223215	0.23127062	0.838101968
8	-13.3593	11.2927	19.0365	0.873446	0.40605134	0.671580641
9	-16.6714	11.4017	16.4564	0.74061984	0.493763579	0.477620243

The computed principal component corresponding to the each response and their multi performance index (MPI) value is given in Table 13. These MPI values are the overall

performance of multiple responses. Optimization was done by Taguchi method as single objective optimization. The main effect plot for data mean is shown in Fig.48, Optimum parameter setting can be found out from the main effect plot. Response table for mean of all MPI are shown in Table 14. Estimated model co efficient for mean is shown in table 15 and analysis of variance table is shown in Table16.

Table.6.7 Computed principal components of (MRR, CW, S) and their respective MPI value

ZNOR SNRA1	ZNOR SNRA2	ZNOR SNRA3	MPI
0.987660678	0.631300971	-0.288199053	0.76954
0.672528216	0.433808606	-0.362070746	0.505531
1.157874385	0.778607244	-0.242477546	0.920698
-0.183145356	0.349127887	-0.086185364	-0.06845
-0.156288519	0.702641503	-0.60681664	-0.04176
0.128659353	1.304815361	-0.151099602	0.324253
0.801775931	0.574953486	0.05658194	0.670528
0.798324949	0.698561689	-0.376557187	0.641886
0.543479965	0.65363107	-0.414233492	0.453211

Table6.8 Response table for mean

Level	v	i	Ton
1	0.9344	0.6527	1.0085
2	0.7222	0.8298	0.6771
3	0.9065	1.0807	0.8776
Delta	0.2122	0.4281	0.3314
Rank	3	1	2

Table6.9 Estimated Model Coefficients for Means

Term	Coef	SE Coef	T	P
Constant	0.85438	0.03804	22.458	0.002
v 22	0.08002	0.05380	1.487	0.275
v 24	-0.13216	0.05380	-2.456	0.133
i 1.0	-0.20173	0.05380	-3.750	0.064
i 1.5	-0.02463	0.05380	-0.458	0.692
Ton 2	0.15408	0.05380	2.864	0.103
Ton 5	-0.17729	0.05380	-3.295	0.081
S=0.1141	R-Sq=95.3%	R-Sq(adj)=81.1%		

Table6.10 ANOVA table for mean

Source	DF	Seq SS	Adj SS	Adj MS	F	P
v	2	0.07976	0.07976	0.03988	3.06	0.246
i	2	0.27762	0.27762	0.13881	10.66	0.086
Ton	2	0.16713	0.16713	0.08356	6.42	0.135
Residual Error	2	0.02605	0.02605	0.01303		
Total	8	0.55056				

R^2 is used to describe the proportion of total variability in the experimental range. From the Table15, it is seen that the R^2 value is 95.3% and adj. R^2 is 81.1%. When R^2 and adj. R^2 differs dramatically there is a good chance of non-significant terms included in the model. R^2 value shows that there is a good amount of reduction in the variability of responses by using input parameters in the model. Hence the developed model is a good regression model. The value of R^2 does not necessarily that imply the regression model is good one. Adding the

variables to the model always increases R^2 regardless whether the additional variable is statically significant or not.

ANOVA was conducted to determine percentage contribution of individual parameters over the performance characteristics. From the table16 it is concluded that current is the most significant factor which affects the responses and voltage affects the least on the performance. No factor is significant within the 95% confidence level.

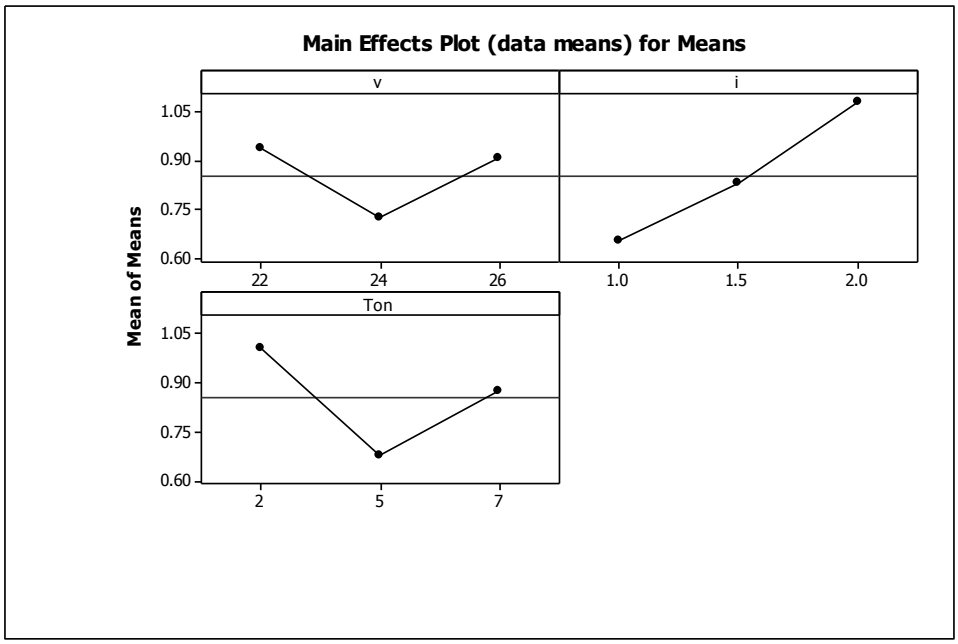

Fig.6.34 Evaluation of optimal parameter setting

Fig.6.27 shows the main effect plot men. At main effects plot graph it is seen that initially with increase of voltage the effect on responses decreases and again effect increases. The effect of current increases continuously as the current increases. The effect of Ton reduces initially and again increases with increasing Ton time.

6.9 Grey relational analysis coupled with PCA results

Eigen analysis of the Correlation Matrix is shown in Table 17 and Table18. These Grey relational grade values are the overall performance of multiple responses in Grey relational grade (Γ) with PCA method; Grey relational grade calculation table is shown in Table 19. Estimated Model Coefficients for Means is shown in table 20. ANOVA Table for means is given in Table 21. Response table for means is shown in Table 22.

Table6.11 Eigen analysis of the Correlation Matrix

Eigenvalue	1.9940	0.7613	0.2447
Proportion	0.665	0.254	0.082
Cumulative	0.665	0.918	1.000

Table6.12 Principal Component of each response

Variable	PC1	PC2	PC3
Ψ 1	0.655	0.091	-0.750
Ψ 2	-0.489	0.808	-0.329
Ψ 3	0.576	0.582	0.574

Table6.13 Grey relational grade with Grey relational coefficient and deviation sequence

Si. No.	Δ0i(1)	Δ0i(2)	Δ0i(3)	Ψ1	Ψ2	Ψ3	Γ
1	0.149686	1	0.211807	0.769603	0.333333	0.702438	0.654053
2	0.210089	0.704675	0.552518	0.704137	0.41505	0.475051	0.612628
3	0	0.72608	0	1	0.407804	1	0.850582
4	1	0.461897	0.941483	0.333333	0.519806	0.346865	0.38214
5	0.650716	0.140983	1	0.434512	0.780051	0.333333	0.514417
6	0.517108	0	0.221031	0.49159	1	0.693451	0.63777
7	0.477678	0.768729	0.161898	0.511416	0.394095	0.755403	0.502135
8	0.126554	0.593949	0.328419	0.798016	0.45706	0.603559	0.696266
9	0.25938	0.506236	0.52238	0.658432	0.496901	0.489055	0.604173

Table6.14 Estimated Model Coefficients for Means

Term	Coef	SE Coef	T	P
Constant	0.85438	0.03804	22.458	0.002
v 22	0.08002	0.05380	1.487	0.275
v 24	-0.13216	0.05380	-2.456	0.133
i 1.0	-0.20173	0.05380	-3.750	0.064
i 1.5	-0.02463	0.05380	-0.458	0.692
Ton 2	0.15408	0.05380	2.864	0.103
Ton 5	-0.17729	0.05380	-3.295	0.081
S = 0.05577	R-Sq=95.6%	R-Sq(adj)=82.3%		

Table6.15 ANOVA for means

Source	DF	Seq SS	Adj SS	Adj MS	F	P
V	2	0.056755	0.056755	0.028378	9.12	0.099
I	2	0.051203	0.051203	0.025601	8.23	0.108
Ton	2	0.026444	0.026444	0.013222	4.25	0.190
Residual Error	2	0.006221	0.006221	0.003110		
Total	8	0.140623				

From the Table20, it is seen that the R^2 value is 95.6% and adj. R^2 is 82.3%. The values of R^2 and adj.R^2 are slightly higher than the WPCA method. Generally adj.R^2 will not always increase, as the variables are added to the model. In fact if unnecessary terms are added, the value of adj. R^2 will often decrease. From Table21 it is concluded that voltage is the most influencing parameter on performance. All the factors are insignificant for 95% confidence interval.

From Fig.6.28 it is concluded that there is a steep decrease of machining performance for some amount of the increase of voltage and then machining performance increases with the increase of voltage within the taken range. Machining performances increases linearly with the increase of current. Machining performance initially reduces for some amount of increase of Ton value and then increases.

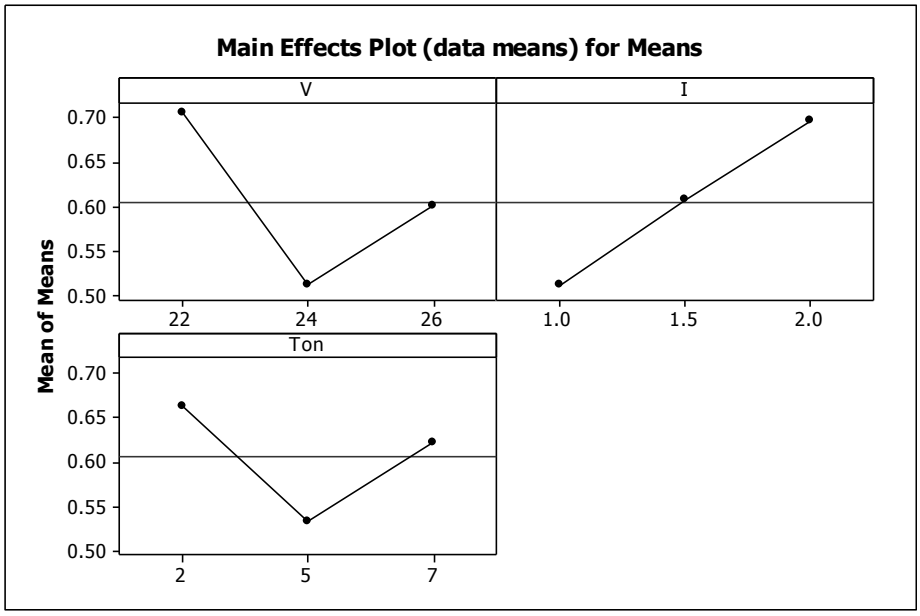

Fig.6.35 Evaluation of optimal parameter setting

6.10 Result of PCA based TOPSIS method

Eigen analysis of the Correlation Matrix is shown in Table22 and Table23. These Grey relational grade values are the overall performance of multiple responses in Grey relational grade (Γ) with PCA method; Grey relational grade calculation table is shown in Table24. Estimated Model Coefficients for Means is shown in table 25. ANOVA Table for means is given in Table 26, and Response table for means is shown in Figure 50.

Table6.16 Eigen analysis of the Correlation Matrix

Eigenvalue	2.1346	0.5900	0.2753
Proportion	0.712	0.197	0.092
Cumulative	0.712	0.908	1.000

Table6.17 Principal Component of each response

Variable	PC1	PC2	PC3
Y1	0.617	0.234	0.751
Y2	-0.521	0.837	0.166
Y3	0.590	0.494	-0.638

Table6.18 Grey relational grade with Grey relational coefficient and deviation sequence

Si. No.	V1	V2	V3	S+	S-	OPI
1	0.6018	0.10724	0.0436	0.4647	2.0268	0.8134
2	0.1694	-0.01019	0.0981	0.8981	1.6214	0.6435
3	0.9871	0.2559	0.0630	0.1109	2.4068	0.9559
4	-1.4095	-0.36124	-0.1568	2.5162	0.6172	0.1969
5	-0.9686	-0.2521	0.0127	2.0515	0.6936	0.2526
6	-0.0832	0.0926	-0.1065	1.1224	1.3372	0.5436
7	0.12046	0.0533	-0.1096	0.9429	1.5441	0.6208
8	0.4844	0.1086	0.0842	0.5627	1.9150	0.7728
9	0.09810	0.0057	0.0713	0.9579	1.5452	0.6173

In Table24, it is seen that R^2 value is 98% and the value of adj. R^2 is 92.0%. The difference between R^2 and adj. R^2 is less compared to the other two optimization methods. Hence there is a less chance of non-significant factors. As R^2 value is 98%, it yields to good prediction of new observations or estimates of mean response. adj. R^2 value shows that there are less unnecessary terms in the model.

Table6.19 Estimated Model Coefficients for Means

Term	Coef	SE Coef	T	P
Constant	0.60192	0.02332	25.811	0.001
v 22	0.20239	0.03298	6.137	0.026
v 24	-0.27081	0.03298	-8.212	0.015
i 1.0	-0.05815	0.03298	-1.763	0.220
i 1.5	-0.04556	0.03298	-1.382	0.301
Ton 2	0.10808	0.03298	3.277	0.082
Ton 5	-0.11598	0.03298	-3.517	0.072
S = 0.06996	R-Sq=98.0%	R-Sq(adj)= 92.0%		

Table 6.20 ANOVA for means

Source	DF	Seq SS	Adj SS	Adj MS	F	P
V	2	0.356956	0.356956	0.178478	36.47	0.027
I	2	0.048643	0.048643	0.024322	4.97	0.168
Ton	2	0.075582	0.075582	0.037791	7.72	0.115
Residual Error	2	0.009789	0.009789	0.004894		
Total	8	0.490970				

From Table25, Voltage is the most significant factor that affects the responses and current is the least significant factors that affect responses. For 95% confidence interval only current is the significant factor.

From Fig.6.29 it is observed that as voltage increases machining performance reduces and gain with increasing further machining performance enhances. Similarly with increasing pulse on time, initially machining performance reduces and with further increasing the value, machining performances increases slightly. With the increase of current, machining performance increases within the working range.

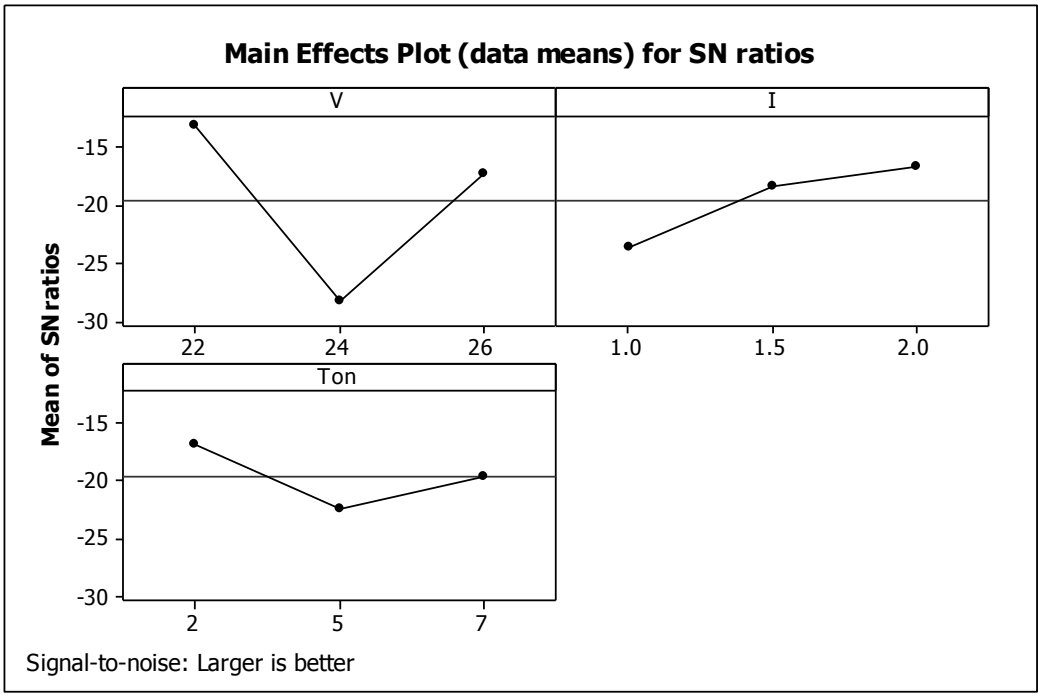

Fig.6.35 Evaluation of optimal parameter setting

CHAPTER 7

Conclusions

- From ANSYS modeling

Thermal modeling was done for INCONEL718 and maximum temperature reached by our model was compared with the earlier developed model. It was seen that maximum temperature reached by our model approaches to the earlier developed model. Then thermal modeling has been done. MRR has been estimated for Aluminum work piece. Modeling has also been done for residual stress. The estimated MRR values were compared with the experimental MRR of Aluminum work piece. The calculated error of MRR lies within the limit of 25%. The temperature profile has been analyzed in the Al work piece material due to high temperature and transient operation. The effect of various process parameters (voltage, current, pulse on time) on temperature distribution for micro WEDM has been discussed.

- From optimization

In the present work three PCA based optimization techniques were applied for optimizing the cutting parameters in micro WEDM of Aluminum work piece. MRR, kerf width and cutting speed are selected as response variables. The research takes account of the correlation between quality characteristics and utilizes the principal component analysis to eliminate the multiple co linearity. The principal component analysis is used to determine the corresponding weights of each response variable.

- In WPCA the optimum cutting parameters are; voltage 22V, current 2.0A and Ton is 2µs.

- In Grey relational coupled with PCA, the optimum cutting parameters are; voltage 22V, Current 2.0A, Ton is 2 µs.
- In PCA based TOPSIS method, the optimum cutting parameters are; voltage 22V, Current 2.0A, Ton is 2 µs.
- Among these three optimization technique, PCA based TOPSIS method is best for optimization of multiple correlated responses.

References

[1] F. Nourbakhsh, “Machining stability of wire EDM of titanium, (2012)" M.S, Industrial and Management System Engineering, University of Nebraska, Nebraska.

[2] D.F. Dauw, C.A. Brown, J.P.V. Griethuysen, J.F.L.M.Albert, (1990) “Surface topography investigations by fractal analysis of spark-eroded, electrically conductive ceramics”, CIRP Annals - Manufacturing Technology 39, pp.161–165.

[3] S.N. Joshi and S.S. Pandey, (2010) “Thermo-Physical modeling of die sinking EDM process”, Journal of Manufacturing Processes 12, pp. 45–56.

[4] M.S. Hewidy, T.A.Taweel, M.F.Safty, (2005) “Modeling the machining parameters of wire electrical discharge machining of Inconel 601 using RSM”, Journal of Materials Processing Technology 169, pp. 328-336.

[5] D. Scott, S. Boyina, K.P. Rajurkar, (2007) “Analysis and optimization of parameter combination in wire electrical discharge machining”, International Journal of Production Research 29, pp.2189-2207.

[6] J.T. Huang, Y.S. Liao, (2010) “Optimization of machining parameters of wire-EDM based on grey relational and statistical analyses”, International Journal of Production Research 41, pp.1707-1720.

[7] T.A. Spedding, Z.Q. Wang, (1997) “Study on modeling of wire EDM process”, Journal of Materials Processing Technology 69, pp 18-28.

[8] K. P. Somashekhar & J.Mathew& N. Ramachandran, (2012) “A feasibility approach by simulated annealing on optimization of micro-wire electric discharge machining parameters”, Int. j. Adv. Manuf. Technology.

[9] M.T. Yan, H.T. Chien, (2007) "Monitoring and control of the micro wire-EDM process", International Journal of Machine Tools and Manufacture 47, pp.148-157.

[10] A. Mohammadi, A.F. Tehrani, E. Emanian, D. Karimi, (2008)"Statistical analysis of wire electrical discharge turning on material removal rate", Materials processing technology 2 0 5, pp.283–289.

[11] T. A. Spedding, Z. Q. Wang ,(1997)"Parametric optimization and surface characterization of wire electrical discharge machining process", Precision Engineering 20, pp.5-15.

[12] S. K Gauri and S. Chakraborty, (2010) "A study on the performance of some multi-response optimization methods for WEDM processes", Int. J Adv. Manuf. Technol. 49:155–166.

[13] S.K Gauri, S. Chakraborty (2009) "Optimization of multiple responses for WEDM processes using weighted principal components", Int. J Adv. Manuf. Technol. 40, pp.1102–1110.

[14] S.H Yeo, W. Kurnia, P.C Tan, (2007)" Critical assessment and numerical comparison of electro-thermal models in EDM", J Mater Process Technol. 203, pp.241-51.

[15] R. Snoeys, F.S.V. Dijck, (1971)"Investigation of electro discharge machining operations by means of thermo-mathematical model". CIRP Ann.20, pp.35-7.

[16] M.R. Patel, M.A. Barrufet, P.T. Eubank, D.D. DiBitonto, (1989) "Theoretical models of the electrical discharge machining process. II. The anode erosion model", Journal of Applied Physics 66, pp.4104-11.

[17] H.K. Kansal, S. Singh, P. Kumar, (2008) "Numerical simulation of powder mixed electric discharge machining (PMEDM) using finite element method". Mathematical and Computational Modeling 47, pp.1217-37.

[18] K.L. Bhondwe, V. Yadava, G. Kathiresan, (2006) "Finite element prediction of material removal rate due to electro chemical spark machining", International journal of machine tool and manufacture 46, pp.1699-1706.

[19] M. Kunieda, B. Lauwers, K.P. Rajurkar, B.M. Schumacher, (2005) "Advancing EDM through fundamental insight into the process", CIRP Ann Manufacturing Technology 54, pp.599-622.

[20] P.C. Pandey, S.T. Jilani, (1986)" Plasma channel growth and the re solidified layer in EDM". Precision Engineering8, pp.104-110.

[21] T.Ikai, K.Hashigushi, (1995)"Heat input for crater formation in EDM". Proceedings of international symposium for electro-machining-ISEM XI, EPFL", pp.163-70.

[22] DONALD B.MOULTON "wire edm the fundamentals" EDM network, Sugar Grove, IL, USA.

[23] A.N.S. Babu, L.K.T, (2012) "Finite element simulation of hybrid welding process for welding 304 austenitic stainless steel plates", Int. J R Engineering and Technology, pp.401-410.

[24] K. Salonitis, A.stournaras, P.Stavropoulos, G. Chryssolouris. (2009) "Thermal modeling of the material removal rate and surface roughness for die-sinking EDM" Int. J. Adv. manufacturing Technology 40, pp.316-323.

[25] MK Pradhan, CK Biswas, (2008), "Modeling of machining Parameters for MRR in EDM using response surface methodology", Proceedings of NCMSTA' 08 Conference, NIT Harripur, India.

[26] A. G. Mamalis, G. C. Vosniakos, N. M. Vaxevanidis, J. Prohaszka,(1987) "Macroscopic and microscopic phenomena of electro-discharge machined steel surfaces: An experimental investigation," Journal of Mechanical Working Technology 15, pp. 335–356.

[27] V. Yadav, V. Jain, P. Dixit, (2002)"Thermal stresses due to electrical discharge machining", Int. J. Machine Tools Manufacturing 42, pp. 877–888.

[28] A. Kumar, (2012) "Modelling of micro wire electro discharge machining (WEDM) in aerospace material," M.Tech, Mechanical Engineering, National Institute of Technology, Rourkela.

[29] T. FU, J. ZHAO, W. LIU, (2012)"Multi-objective optimization of cutting parameters in high-speed milling based on grey relational analysis coupled with principal component analysis", Front. Mechanical Engineering 7, pp.445-452.

[30] L.I. Tong, C.H.Wang, H.C. Chen,(2005)" Optimization of multiple responses using principal component analysis and technique for order preference by similarity to ideal solution " Int. J Adv. Manufacturing Technology 27, pp.407-414.

[31] H.C. Liao, (2006)" Multi-response optimization using weighted principal component", Int. J Adv. Manufacturing Technology 27, pp.720-725.

[32] S. Das and S. S. Joshi,(2010)" Modeling of spark erosion rate in micro wire-EDM", Int. J Adv. Manufacturing Technology 48, pp.551-596.

[33] M. Malik, R. K. Yadav, N. K.,D.Sharma,(2012)" optimization of process parameters of wire edm using zinc-coated brass wire", International Journal of Advanced Technology & Engineering Research, ISSN No: 2250-3536.

[34] R.V.Rao, P.J.Pawar, (2010), "Process parameter modeling and optimization of Wire Electrical Discharge Machining", advances in production engineering and management 5, pp.138-200.

[35] S. Datta,S. S. Mahapatra,(2010), "Modeling, simulation and parametric optimization of wire EDM process using response surface methodology coupled with grey-Taguchi technique " International Journal of Engineering, Science and Technology 5, pp. 162-183.

[36] P. Gupta, R.Khanna, R. Dev Gupta, N. Sharma," Effect of Process Parameters on Kerf Width in WEDM for HSLA Using Response Surface Methodology" journal of engineering and technology2, pp.1-6.

[37] N. Sharma, R. khanna," Optimization of process parameters of cryogenic treated D-3 in WEDM by Taguchi Approach" IJERA 1 , pp.546-553.

[38] T. P. S. Inbaraj, M. Vinoth," dynamic analysis of milling machine chatter vibration reduction using mechanical damper by FEA", Journal of Mechanical Sciences 1, pp. 48-58.

[39] S.D.Lahane, M.K.Rodgr, S.B. Sharma, (2012)" Multi-response optimization of Wire-EDM process using principal component analysis", IOSR Journal of Engineering, pp. 38-47.

[40] http://en.wikipedia.org/wiki/Wire_cutting#Wire_EDM.

[41] Sorabh, M.Kumar, N. Nirmal, (2013) “a literature review on optimization of machinin1g parameters in wire EDM”, International Journal of Latest Research in Science and Technology 2, pp.492-494.

[42] B. C. Routara, B.K. Nanda, D.R.Patra, (2009) ” Parametric optimization of CNC wire cut EDM using grey relational analysis”, International Conference on Mechanical Engineering.

[43] A.N. Siddiquee, Z.A. Khan, Z. Mallick, (2010)” Grey relational analysis coupled with principal component analysis for optimization design of the process parameters in in-feed Centre less cylindrical grinding” The International Journal of Advanced Manufacturing Technology 46, pp. 983-992.